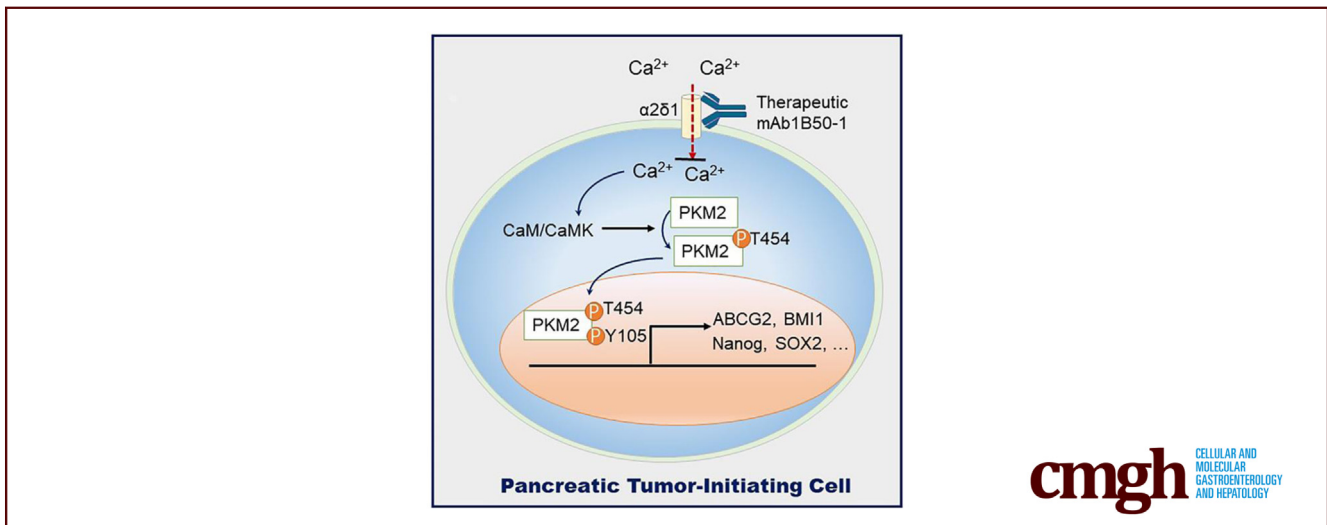


## ORIGINAL RESEARCH

Calcium Channel  $\alpha 2\delta 1$  is Essential for Pancreatic Tumor-Initiating Cells through Sequential Phosphorylation of PKM2Jingtao Liu,<sup>1,2,\*</sup> Ming Tao,<sup>3,\*</sup> Wei Zhao,<sup>1,\*</sup> Qingru Song,<sup>1</sup> Xiaodan Yang,<sup>1</sup> Meng Li,<sup>1</sup> Yanhua Zhang,<sup>2,§</sup> Dianrong Xiu,<sup>3,§</sup> and Zhiqian Zhang<sup>1,§</sup>

<sup>1</sup>Key Laboratory of Carcinogenesis and Translational Research, (Ministry of Education/Beijing), Department of Cell Biology, Peking University Cancer Hospital and Institute, Beijing, P.R. China; <sup>2</sup>Department of Pharmacology, Peking University Cancer Hospital and Institute, Beijing, P.R. China; and <sup>3</sup>Department of General Surgery, Peking University Third Hospital, Beijing, P.R. China



## SUMMARY

Voltage-gated calcium channel  $\alpha 2\delta 1$  was identified as a functional marker and therapeutic target of pancreatic tumor-initiating cells. It mediated calcium influx to activate CaMKII $\delta$ , which phosphorylated PKM2 at Thr454 that led to subsequent PKM2- Tyr105 phosphorylation, to induce stem-like properties.

**BACKGROUND & AIMS:** Tumor-initiating cells (TICs) drive pancreatic cancer tumorigenesis, therapeutic resistance, and metastasis. However, TICs are highly plastic and heterogeneous, which impede the robust identification and targeted therapy of such a population. The aim of this study is to identify the surface marker and therapeutic target for pancreatic TICs.

**METHODS:** We isolated voltage-gated calcium channel  $\alpha 2\delta 1$  subunit (isoform 5)-positive subpopulation from pancreatic cancer cell lines and freshly resected primary tissues by fluorescence-activated cell sorting and evaluated their TIC properties by spheroid formation and tumorigenic assays. Coimmunoprecipitation was used to identify the direct substrate of CaMKII $\delta$ .

**RESULTS:** We demonstrate that the voltage-gated calcium channel  $\alpha 2\delta 1$  subunit (isoform 5) marks a subpopulation of

pancreatic TICs with the highest TIC frequency among the known pancreatic TIC markers tested. Furthermore,  $\alpha 2\delta 1$  is functionally sufficient and indispensable to promote TIC properties by mediating  $\text{Ca}^{2+}$  influx, which activates CaMKII $\delta$  to directly phosphorylate PKM2 at T454 that results in subsequent phosphorylation at Y105 to translocate into nucleus, enhancing the stem-like properties. Interestingly, blocking  $\alpha 2\delta 1$  with its specific antibody has remarkably therapeutic effects on pancreatic cancer xenografts by reducing TICs.

**CONCLUSIONS:**  $\alpha 2\delta 1$  promotes pancreatic TIC properties through sequential phosphorylation of PKM2 mediated by CaMKII $\delta$ , and targeting  $\alpha 2\delta 1$  provides a therapeutic strategy against TICs for pancreatic cancer. (*Cell Mol Gastroenterol Hepatol* 2023;15:373–392; <https://doi.org/10.1016/j.jcmgh.2022.10.006>)

**Keywords:** Pancreatic Cancer; Tumor-Initiating Cell; Therapeutic Target.

Pancreatic ductal adenocarcinoma (PDAC) is the major type of pancreatic cancer, which represents one of the most common and deadly cancers with a relative 5-year survival rate less than 10%.<sup>1,2</sup> The poor prognosis of PDAC is believed to be attributed to late detection, aggressive behavior, heterogeneity, and therapeutic resistance of

the disease. Although early detection is undoubtedly critical for the survival of PDAC patients, a better understanding of the biology of PDAC associated with its progression is also imperative for the development of more efficient therapeutic strategies.<sup>3</sup>

As a subpopulation of cancer cells with stem cell-like properties such as self-renewal, differentiation, and tumorigenic capacity, tumor-initiating cells (TICs), or so-called cancer stem cells, have the ability to recapitulate the whole heterogeneity of a tumor and therefore are postulated as a sustaining force to drive and maintain fully malignancy of a tumor.<sup>4,5</sup> Targeting these cells thus is expected to bring a “cure” for the patients. Although several surface markers such as CD133, CD44, EpCAM, DCLK1, and CD9<sup>6-8</sup> have been used to define TICs for PDAC in literature, the reliable identification of such a population in PDAC is hampered by the need for specific markers that can be used for isolation and clinical targeting.

The auxiliary subunit of voltage-gated calcium channels (VGCC)  $\alpha 2\delta 1$  is a product of single gene that is post-translationally cleaved into  $\alpha 2$  and  $\delta 1$  subunits, which subsequently form a dimer via disulfide bonds. It can promote membrane expression of VGCC and modulate its current properties by interacting with the core forming  $\alpha 1$  subunit.<sup>9</sup> A change in voltage moves the switch that in turn pulls the “gate” of the channel open, which subsequently leads to influx of calcium ions ( $\text{Ca}^{2+}$ ) into cells.<sup>10</sup> By serving as a major second messenger, elevated  $\text{Ca}^{2+}$  in the cells relays signals in the form of spikes or oscillations, which are decoded by several downstream sensor and adaptor proteins including calmodulin (CaM), to control a variety of cellular processes including gene transcription, cell metabolism, proliferation, motility, cell death, and survival.<sup>10,11</sup>  $\text{Ca}^{2+}$ /CaM complex subsequently binds and activates a number of downstream enzymes such as the  $\text{Ca}^{2+}$ /CaM-dependent protein kinase II (CaMKII), a multifunctional serine/threonine kinase family of 4 closely related isoforms (CaMKII $\alpha$ ,  $\beta$ ,  $\gamma$ , and  $\delta$ ) that show differential but overlapping expression patterns among tissues and during development.<sup>12,13</sup> As one of the most widely studied  $\text{Ca}^{2+}$ -regulated kinases, CaMKII comprises 12 identical subunits that form a dodecameric holoenzyme. Activation of individual subunits of the holoenzyme by  $\text{Ca}^{2+}$ /CaM leads to the phosphorylation of adjacent enzyme subunits at Thr286/287 (the  $\alpha$  isoform at Thr286, the  $\beta$ ,  $\gamma$ , and  $\delta$  isoforms at Thr287). Once autophosphorylated, CaMKII acquires enhanced enzymatic activity that remains even after  $\text{Ca}^{2+}$ /CaM dissociation.<sup>14,15</sup>

Breakdown of  $\text{Ca}^{2+}$  homeostasis and/or aberrant expression of calcium signaling pathway molecules have been linked to many pathologic processes including cancer.<sup>10,12,16</sup> Extensive remodeling in the expression of proteins and/or the activity directly involved in calcium signaling have been observed as consequences of oncogenic pathways. On the other hand, many oncogenic machineries are sensitive to the regulation by specific calcium signal(s) that can initiate the formation of some cancers, promote tumor cell growth, angiogenesis, migration, invasion, and metastasis, prevent tumor cell death, as well as regulate the response to therapeutic agents and the acquisition of therapeutic

resistance.<sup>16-18</sup> Recently, a number of studies indicated that changes in intracellular calcium ( $[\text{Ca}^{2+}]_i$ ) also play essential roles in the self-renewal capacity and differentiation of stem cells and cancer stem cells, as results of the expression of a wide variety of calcium channels such as VGCC and/or store release channels (IP3R and RYR).<sup>18-20</sup> We have previously identified that the isoform 5 of the VGCC  $\alpha 2\delta 1$  subunit, which is specifically recognized by the monoclonal antibody (mAb) 1B50-1, is sufficient and indispensable to promote TIC properties by mediating  $\text{Ca}^{2+}$  influx into cells, hence serving as a functional marker and therapeutic target of TICs of liver,<sup>21,22</sup> lung,<sup>23</sup> and gastric<sup>24</sup> origins. However, the calcium signaling pathways mediated by  $\alpha 2\delta 1$  in the determination of TIC properties remain elusive.

PKM2 is the M2 isoform of pyruvate kinase (PK) that regulates the final rate-limiting step of glycolysis by transferring the phosphate from phosphoenolpyruvate to adenosine diphosphate to generate pyruvate and adenosine triphosphate.<sup>25</sup> In addition to its role in glycolysis, PKM2 can function as a protein kinase or a transcriptional co-activator to activate the transcription of those genes that are essential for tumorigenesis.<sup>26-29</sup> Moreover, the roles of PKM2 in oncogenesis are dependent on its posttranslational modification. For example, the phosphorylation of PKM2 at Tyr105 (Y105) by multiple tyrosine kinases results in the formation of PKM2 dimers that induce cancer stem cell-like properties in human breast cancer by enhancing Yes-associated protein (YAP) nuclear translocation.<sup>28</sup>

Here, we show that  $\alpha 2\delta 1$  is a functional marker and therapeutic target for pancreatic cancer TICs. The expression of  $\alpha 2\delta 1$  is sufficient to induce stem-like properties via  $\text{Ca}^{2+}$ -mediated activation of CaMKII $\delta$ , which directly phosphorylates PKM2 at T454 that subsequently resulted in the phosphorylation of PKM2 at Y105 in a sequential mode. Importantly, blocking calcium influx with mAb1B50-1 against  $\alpha 2\delta 1$  can selectively reduce TICs, providing a promising approach of targeted therapy for pancreatic cancer.


## Results

### $\alpha 2\delta 1$ Defines a TIC Subpopulation of PDAC

To test whether  $\alpha 2\delta 1$  marks a subpopulation of TICs in PDAC, we first detected the expression of  $\alpha 2\delta 1$  in the PDAC

\*Authors share co-first authorship; §Authors share co-corresponding authorship.

**Abbreviations used in this paper:** CaM, calmodulin; FACS, fluorescence-activated cell sorting; GEM, gemcitabine; i.p., intraperitoneally; IRS, immunoreactive score; mAb, monoclonal antibody; NOD/SCID, nonobese diabetic/severe combined immunodeficient; OE, overexpression; PDAC, pancreatic ductal adenocarcinoma; PDX, patient-derived xenograft; PK, pyruvate kinase; s.c., subcutaneously; SDS-PAGE, sodium dodecyl sulfate-polyacrylamide gel electrophoresis; shRNA, short hairpin RNA; TIC, tumor-initiating cell; VGCC, voltage-gated calcium channels; YAP, Yes-associated protein.

 Most current article

© 2022 The Authors. Published by Elsevier Inc. on behalf of the AGA Institute. This is an open access article under the CC BY-NC-ND license (<http://creativecommons.org/licenses/by-nc-nd/4.0/>).

2352-345X

<https://doi.org/10.1016/j.jcmgh.2022.10.006>

cell lines PANC-1 and BxPC-3, as well as the normal human pancreatic duct cell line HPDE6-C7 by immunofluorescent cytochemistry with mAb1B50-1. As shown in Figure 1A,  $\alpha 2\delta 1$  localized in the cell membrane of a minor population in the PDAC cell lines, whereas it is undetectable in the immortalized normal pancreatic duct cell line HPDE6-C7. The percentage of  $\alpha 2\delta 1$ -positive ( $\alpha 2\delta 1^+$ ) cells varied from 1.33% to 4.66% across a panel of PDAC cell lines including AsPC-1, BxPC-3, MIA PaCa-2, and PANC-1 as detected by flow cytometry (Figure 1B). Furthermore, the  $\alpha 2\delta 1^+$  cells stained by 1B50-1 were confirmed to be positive for a commercial  $\alpha 2\delta 1$  antibody by both immunofluorescent cytochemistry and flow cytometry (Figure 1C and D). We then performed fluorescence-activated cell sorting (FACS) to purify  $\alpha 2\delta 1^+$  and  $\alpha 2\delta 1^-$  cells from these PDAC cell lines to assay their cancer stem cell capacities both in vitro and in vivo. Sorted  $\alpha 2\delta 1^+$  cells from these PDAC cell lines could form spheres at much higher rates than their respective negative subsets in serum-free medium (Figure 1E and F). Single cells dissociated from the spheres formed by these  $\alpha 2\delta 1^+$  cells could be passaged and clonally expanded with enhanced sphere formation efficiencies, suggesting that the  $\alpha 2\delta 1^+$  cells possess the in vitro self-renewal capacity (Figure 1E and F). The FACS-purified  $\alpha 2\delta 1^+$  and  $\alpha 2\delta 1^-$  cells were then serially transplanted in nonobese diabetic/severe combined immunodeficient (NOD/SCID) mice subcutaneously (s.c.) at serial dilutions of 1000 and 100 cells to assay their tumorigenicity. The  $\alpha 2\delta 1^+$  subpopulations from these cell lines generated tumors in almost all the transplanted mice, whereas the respective  $\alpha 2\delta 1^-$  cells were either completely non-tumorigenic or formed tiny nodules only occasionally. Furthermore,  $\alpha 2\delta 1^+$  subpopulations re-sorted from the tumors formed by the  $\alpha 2\delta 1^+$  cells were able to generate tumors in the secondary recipient mice (Figure 1G, Table 1). The histopathologic features of the tumors formed by the  $\alpha 2\delta 1^+$  cells resembled those of the tumors formed by which the  $\alpha 2\delta 1^+$  cells originated as demonstrated by H&E staining (Figure 1H), suggesting that  $\alpha 2\delta 1^+$  cells were able to initiate the formation of the heterogeneous tumors they derived.

In addition, the  $\alpha 2\delta 1^+$  cells expressed much higher levels of a panel of stem-associated molecules, eg, ABCG2, BMI1, NANOG, SOX2, than their negative ones as demonstrated by Western blotting (Figure 1I). It was hypothesized that TICs could undergo asymmetric cell division that resulted in the production of a stem cell and a progenitor cell, the latter of which could differentiate into non-TICs.<sup>18,30</sup> Hence, we detected whether sorted  $\alpha 2\delta 1^+$  cells were able to generate  $\alpha 2\delta 1^-$  cells both in vitro and in vivo. The percentage of  $\alpha 2\delta 1^+$  fractions purified from both the PANC-1 and BxPC-3 cell lines decreased from about 90% to 2%–5%, which were similar to those in parent cell lines, after the purified  $\alpha 2\delta 1^+$  cells were cultivated in medium containing 10% fetal bovine serum for 2 weeks or transplanted into NOD/SCID mice (Figure 1J), suggesting the differentiation ability of  $\alpha 2\delta 1^+$  into negative ones. On the contrary, the  $\alpha 2\delta 1^-$  cells purified from both cell lines failed to differentiate into  $\alpha 2\delta 1^+$  cells after being cultured in serum-containing medium for 2 weeks (Figure 1K).

All of these data confirmed that the VGCC  $\alpha 2\delta 1$  marked a TIC subpopulation with stem-like properties of pancreatic cancer.

### *TICs Are Enriched the Most in $\alpha 2\delta 1^+$ Cells among $CD9^+$ , $CD44^+$ , $EpCAM^+$ , and $DCLK1^+$ Ones*

To further characterize the  $\alpha 2\delta 1^+$  PDAC TICs, we determined the correlation between  $\alpha 2\delta 1$  and CD9, CD44, EpCAM, or DCLK1, the surface markers that have been used to isolate PDAC TICs, in the PDAC cell lines PANC-1 and BxPC-3 by dual-color flow cytometry. More than 90% of  $\alpha 2\delta 1^+$  cells were also positive for CD9, CD44, EpCAM, and DCLK1, whereas less than one third (3.5%–31.1%) of  $CD9^+$ ,  $CD44^+$ ,  $EpCAM^+$ , or  $DCLK1^+$  subpopulations were positive for  $\alpha 2\delta 1$  in both PANC-1 and BxPC-3 cell lines (Figure 2A and B), indicating that  $\alpha 2\delta 1^+$  TICs are a shared subpopulation of the pancreatic cancer TICs defined by these known markers.

We then sought to address which marker was the best to identify TICs of PDAC by carrying out a side-by-side comparison of the tumorigenic potential among  $\alpha 2\delta 1^+$ ,  $CD9^+$ ,  $CD44^+$ ,  $EpCAM^+$ , and  $DCLK1^+$  PANC-1 cells in NOD-SCID mice with limited dilution. Compared with those of  $CD44^+$ ,  $EpCAM^+$ , and  $DCLK1^+$  fractions, the TIC frequencies of  $\alpha 2\delta 1^+$  cells were 11.09, 11.09, and 37.9 times those of  $CD44^+$ ,  $EpCAM^+$ , and  $DCLK1^+$  cells, respectively (Figure 2C, Table 2). In another experiment set, the TIC frequency of  $\alpha 2\delta 1^+$  cells was about 1000 times that of  $CD9^+$  fraction (Figure 2D, Table 2). These data indicate that  $\alpha 2\delta 1$  is the most robust surface marker for defining PDAC TICs among these molecules tested.

### *Clinical Significance of $2\delta 1^+$ Cells in Pancreatic Cancer and Surgical Margin Tissues*

To address the clinical relevance of  $\alpha 2\delta 1$  expression in pancreatic cancer, we performed immunofluorescent staining in 74 paired frozen pancreatic cancer and paracancerous tissues that were obtained from the pancreatectomy margins using mAb1B50-1. The cells positive for  $\alpha 2\delta 1$  staining, which were also positive for CK19 staining, showed a scattered distribution in 89.2% (66/74) of all the pancreatic cancer tissues tested, whereas they were detected only as isolated ones in 59.5% (44/74) of paracancerous tissues (Figure 3A). Both the  $\alpha 2\delta 1^+$  and  $\alpha 2\delta 1^-$  fractions were then sorted directly from freshly resected PDAC tissues of 6 patients and were assayed for their tumorigenic potential. As few as 1000  $\alpha 2\delta 1^+$  cells purified from the fresh tumor tissues were able to generate tumors in 4 of 6 cases tested, whereas no tumor formation was observed for the  $\alpha 2\delta 1^-$  cells isolated from the same tissues in all the transplanted mice (Figure 3B). H&E staining demonstrated that the histologic features of tumors formed by the  $\alpha 2\delta 1^+$  fractions also resembled those from which they derived, retaining the phenotypic heterogeneity (Figure 3C).

Kaplan-Meier curves showed that the  $\alpha 2\delta 1$  staining status in the tumor tissues did not correlate with overall survival of these patients, but the median overall survival in the patients

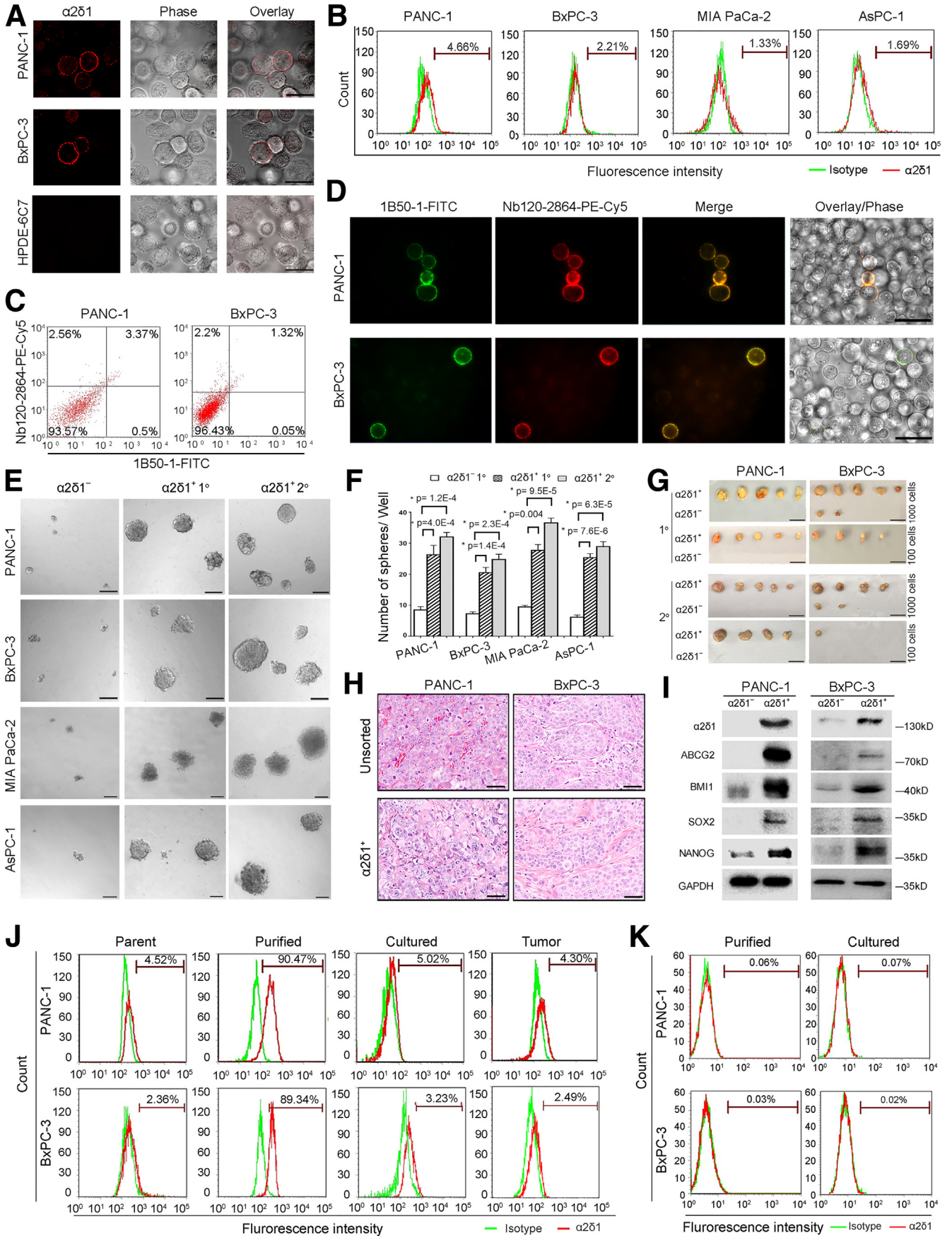


**Table 1.** Tumorigenicity of  $\alpha 2\delta 1^+$  and  $\alpha 2\delta 1^-$  PDAC Cells in NOD/SCID Mice

Cells	$\alpha 2\delta 1$	Tumor formation		Frequency of tumorigenic cells (95% CI)	P value
		1000	100		
PANC-1	Positive	5/5	5/5	1 (1/125–1)	5.4E-10 <sup>a</sup>
	Negative	0/5	0/5	1/ $\infty$ (1/ $\infty$ –1/1836)	
ST	Positive	5/5	4/4	1 (1/156–1)	5.6E-9 <sup>a</sup>
	Negative	0/5	0/4	1/ $\infty$ (1/ $\infty$ –1/1803)	
BxPC-3	Positive	5/5	4/5	1/62.6 (1/185–1/21.4)	2.6E-5 <sup>a</sup>
	Negative	2/5	0/5	1/2212 (1/8821–1/555)	
ST	Positive	4/5	2/5	1/452 (1/1205–1/170)	0.0077 <sup>a</sup>
	Negative	1/5	0/5	1/4983 (1/35191–1/706)	
MIA PaCa-2	Positive	4/5	5/5	1/235 (1/727–1/76)	9.5E-4 <sup>a</sup>
	Negative	1/5	1/5	1/2458 (1/10394–1/581)	
AsPC-1	Positive	4/5	4/5	1/289 (1/839–1/100)	6.9E-4 <sup>a</sup>
	Negative	1/5	0/5	1/4983 (1/35191–1/706)	

ST, serial transplantation.

<sup>a</sup>Compared with the respective  $\alpha 2\delta 1$  negative counterparts.

with  $\alpha 2\delta 1$  negative staining in the paracancerous tissues was 7.5 months longer than those with positive staining (Figure 3D and E). Multi-variant Cox regression analysis showed the presence of  $\alpha 2\delta 1^+$  cells in paracancerous tissues was an independent risk factor of poor prognosis for PDAC patients (Figure 3F).

### Roles of $\alpha 2\delta 1$ in the Acquisition and Subsequent Maintenance of TIC Properties

To test whether  $\alpha 2\delta 1$  plays any roles in the determination of the properties of PDAC TICs, we performed both gain-of-function and loss-of-function studies. Ectopic expression of  $\alpha 2\delta 1$  in the pancreatic cancer cell lines PANC-1 and BxPC-3 led to significant up-regulation of a panel of stem-related genes and remarkably increased the ability of initiating the formation of spheroids that could be expanded in subsequent propagation (Figure 4A–C). On the contrary, knockdown of  $\alpha 2\delta 1$  with short hairpin RNAs (shRNAs) in  $\alpha 2\delta 1^+$  cells resulted in remarkable down-regulation of the stem-related genes detected (Figure 4D), the suppression of spheroid formation abilities (Figure 4E and F), as well as the retardation of tumorigenicity (Figure 4G and H). The role of  $\alpha 2\delta 1$  in the

acquisition and subsequent maintenance of in vitro self-renewal ability of PDAC TICs was further validated in the AsPC-1 and MIA PaCa-2 cell lines by spheroid formation assay (Figure 4B, C, E, and F).

All these data confirmed that  $\alpha 2\delta 1$  is sufficient to enable pancreatic cancer cells to acquire the stem-like properties and is necessary for the subsequent maintenance of pancreatic cancer TIC properties.

### Role of $\alpha 2\delta 1$ in Promoting TIC Properties Is CaMKII $\delta$ -Dependent

Many of the previous studies have linked  $\alpha 2\delta 1$  to its role in mediating calcium influx into cells.<sup>9,22,23</sup> Here, we confirmed that forced expression of  $\alpha 2\delta 1$  led to significantly elevated levels of  $[Ca^{2+}]_i$  in the pancreatic PANC-1 and BxPC-3 cell lines, and that the  $[Ca^{2+}]_i$  levels were much higher in the  $\alpha 2\delta 1^+$  fractions than their negative ones (Figure 5A and B). Further treatment of  $\alpha 2\delta 1^+$  PANC-1 and BxPC-3 cells with 10  $\mu\text{mol/L}$  EGTA-AM could completely inhibit the sphere formation ability of these cells (Figure 5C and D), indicating that the in vitro self-renewal ability of  $\alpha 2\delta 1^+$  cells was dependent on intracellular calcium. To delineate the signaling pathway(s) mediated by calcium in the determination of pancreatic TICs, we focused on the members of  $Ca^{2+}/CaM$ -

**Figure 1. (See previous page). The  $\alpha 2\delta 1^+$  pancreatic cancer cells own stem cell-like properties.** (A) Immunofluorescent staining for  $\alpha 2\delta 1$  with mAb1B50-1 in living cells of indicated cell lines. Scale bars: 25  $\mu\text{m}$ . (B) Flow cytometry analysis of  $\alpha 2\delta 1^+$  fractions in indicated PDAC cell lines. (C) Relationship between  $\alpha 2\delta 1^+$  cells stained by mAb1B50-1-FITC and those stained by PE-Cy5-labeled commercial anti- $\alpha 2\delta 1$  antibody (Novus; Nb120-2864). (D) Representative micrographs demonstrating localization of  $\alpha 2\delta 1$  epitopes in indicated cells stained by 1B50-1-FITC and PE-Cy5-labeled commercial mouse anti- $\alpha 2\delta 1$  monoclonal antibody (Nb120-2864). Scale bars: 25  $\mu\text{m}$ . (E and F) Representative phase contrast micrographs (E) and histograms (F) showing primary (1 $^\circ$ ) and serially passaged (2 $^\circ$ ) spheroids formed by indicated subpopulations purified from indicated cell lines. Data represent mean  $\pm$  standard deviation of 3 independent experiments. \*Two-tailed Student *t* test. Scale bars: 100  $\mu\text{m}$ . (G) Photographs showing dissected tumors formed by sorted  $\alpha 2\delta 1^+$  and  $\alpha 2\delta 1^-$  cells from indicated sources. Bar = 1 cm. (H) Histology of tumors formed by  $\alpha 2\delta 1^+$  cells sorted from indicated sources was compared with that of tumors formed by the respective parent cell lines as demonstrated by H&E staining. Scale bars: 50  $\mu\text{m}$ . (I) Western blot analysis of expression of indicated molecules in FACS-purified  $\alpha 2\delta 1^+$  and  $\alpha 2\delta 1^-$  fractions from indicated cell lines. (J) Flow cytometry analysis of percentage of  $\alpha 2\delta 1^+$  fractions in parental cells (Parent), freshly FACS-purified  $\alpha 2\delta 1^+$  subpopulations (Purified), and purified  $\alpha 2\delta 1^+$  cells cultured in 10% fetal bovine serum for 2 weeks (Cultured) or engrafted into NOD/SCID mice (Tumor). (K) Percentage of  $\alpha 2\delta 1^+$  fractions was analyzed by flow cytometry in FACS-sorted  $\alpha 2\delta 1^-$  subpopulations (Purified) and purified  $\alpha 2\delta 1^-$  cells cultured in 10% fetal bovine serum for 2 weeks (Cultured).

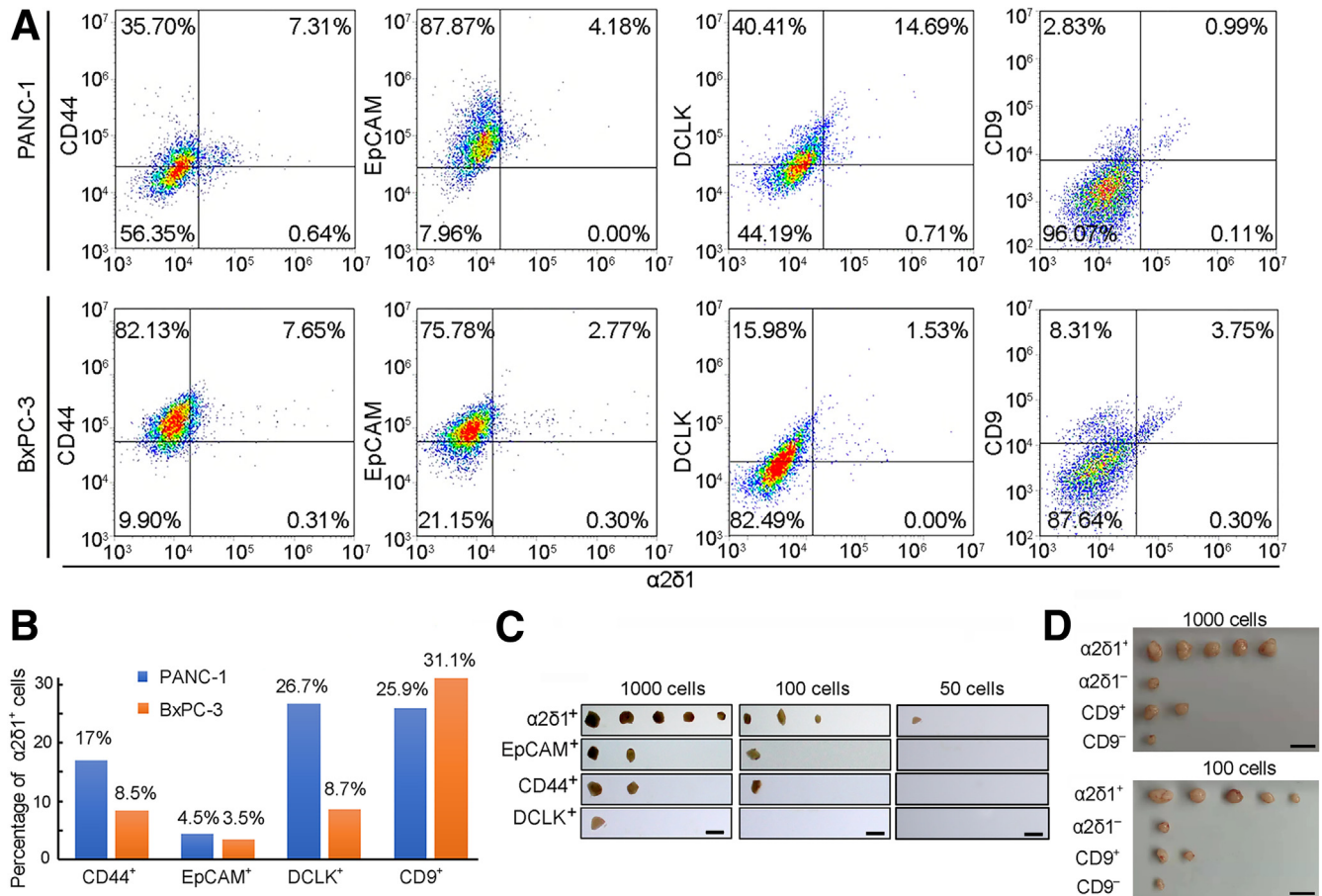


**Figure 2. Characterization of  $\alpha 2\delta 1^+$  TICs of PDAC.** (A) Relationship between expression of  $\alpha 2\delta 1$  and that of indicated molecules was detected by flow cytometry in PANC-1 and BxPC-3 cell lines. (B) Percentage of  $\alpha 2\delta 1^+$  fractions in indicated subpopulations of PDAC cell lines. (C and D) Tumorigenicity of indicated fractions sorted from PANC-1 cell line was compared side-by-side in 2 independent experiment sets. Bar = 1 cm.

dependent protein kinase II family, one of the critical calcium decoders. Of the 4 members of CaMKII, CaMKII $\delta$  was found to be the most dominantly and consistently up-regulated isoform after forced expression of  $\alpha 2\delta 1$  in both the PANC-1 and BxPC-3 cell lines, as demonstrated by Western blotting (Figure 5E). Moreover, the level of phosphorylated CaMKII at Thr286/287 was also up-regulated following  $\alpha 2\delta 1$  overexpression, suggesting the activation of CaMKII (Figure 5E). In addition, the expression of CaMKII $\delta$  was much higher in the  $\alpha 2\delta 1^+$  fractions than their negative ones (Figure 5F). Knockdown of the expression of CaMKII $\delta$  with its specific shRNAs in the  $\alpha 2\delta 1$  overexpressing (OE) cells resulted in down-regulation of stem-related genes detected, significant retardation of spheroid formation efficiencies and tumorigenicity (Figure 5G–J, Table 3). Further knockdown of the expression of CaMKII $\delta$  in the purified  $\alpha 2\delta 1^+$  TICs led to similar effects with the down-regulation of the same panel of stem-related genes and suppression of the abilities of sphere formation and tumorigenicity (Figure 5K–N, Table 3). These results indicate that CaMKII $\delta$  is required for  $\alpha 2\delta 1$ -mediated acquisition and subsequent maintenance of the properties of pancreatic TICs.

#### CaMKII $\delta$ Directly Phosphorylates PKM2 at T454

We then performed immunoprecipitation with anti-FLAG M2 beads in the cell lysates of 293FT cells transiently transfected with CaMKII $\delta$ -Flag construct to identify potential substrate(s) of CaMKII $\delta$  that were involved in the TIC properties promoted by  $\alpha 2\delta 1$ . Compared with the anti-FLAG M2 beads incubated with the cell lysates of 293FT cells transfected with empty control vector, the anti-FLAG M2 beads incubated with the CaMKII $\delta$ -Flag cell lysates precipitated CaMKII $\delta$  itself as expected, and several other top candidates including PKM2, whose phosphorylation at Y105 has been demonstrated as inducing cancer stem cell-like phenotypes in human breast cancer,<sup>28</sup> as revealed by mass spectrometry analyses of the bands indicated in Figure 6A, and thus was selected for further characterization. The physiological binding between CaMKII $\delta$  and PKM2 was verified by carrying out co-immunoprecipitation of extracts from PANC-1 cells overexpressing  $\alpha 2\delta 1$  with antibodies against CaMKII $\delta$  and PKM2. As expected, PKM2 was co-immunoprecipitated by antibody against CaMKII $\delta$  and vice versa (Figure 6B), demonstrating that the 2 proteins bind each other specifically.

**Table 2.** Tumorigenicity of the Indicated Fractions FACS-Purified from the PANC-1 Cell Line in NOD/SCID Mice

Makers	Tumor formation			Frequency of tumorigenic cells (95% CI)	P value
	1000	100	50		
Set 1 experiment					
$\alpha 2\delta 1^+$	5/5	3/5	1/5	1/138 (1/361–1/53.3)	
EpCAM <sup>+</sup>	2/5	1/5	0/5	1/1531 (1/474.1–1/4946)	8.9E-04 <sup>a</sup>
CD44 <sup>+</sup>	2/5	1/5	0/5	1/1531 (1/474.1–1/4946)	8.9E-04 <sup>a</sup>
DCLK1 <sup>+</sup>	1/5	0/5	0/5	1/5235 (1/744.3–1/36831)	2.3E-05 <sup>a</sup>
Set 2 experiment					
$\alpha 2\delta 1^+$	5/5	5/5	ND	1 (1/125–1)	
$\alpha 2\delta 1^-$	1/5	1/5	ND	1/2458 (1/10394–1/581)	1.6E-07 <sup>a</sup>
CD9 <sup>+</sup>	2/5	2/5	ND	1/1061 (1/3128–1/360)	4.7E-06 <sup>a</sup>
CD9 <sup>-</sup>	1/5	1/5	ND	1/2458 (1/10394–1/581)	1.6E-07 <sup>a</sup>

ND, not done.

<sup>a</sup>Compared with the respective  $\alpha 2\delta 1^+$  fractions of each set of experiments.

We next performed mass spectrometry analyses for the phosphorylation site(s) of PKM2 immunoprecipitated from  $\alpha 2\delta 1$ -OE PANC-1 cells. The phosphorylation of PKM2 at T454 was identified in the immunoprecipitated products from the  $\alpha 2\delta 1$ -OE cells (Figure 6C and D). Further Western blot using a site-specific antibody against phosphorylated PKM2 at T454 (Phospho-PKM2-T454, p-PKM2-T454) confirmed that the phosphorylation levels of PKM-T454 were much higher in the  $\alpha 2\delta 1$ -OE and  $\alpha 2\delta 1^+$  PANC-1 and BxPC-3 cells than the respective vector alone control cells and sorted  $\alpha 2\delta 1^-$  subpopulations, respectively, whereas the total PKM2 remained the same (Figure 6E). Ectopic expression of CaMKII $\delta$  in PANC-1 cells also dramatically led to this phosphorylation, whereas the construct CaMKII $\delta$  with T287A mutation that led to the disruption of the kinase activity failed to induce such phosphorylation (Figure 6F). Treatment of  $\alpha 2\delta 1$ -OE PANC-1 cells with KN-93, a specific inhibitor of CaMKII, could remarkably decrease the levels of phosphorylated PKM2-T454 in a dose-dependent manner (Figure 6G). Furthermore, knockdown of CaMKII $\delta$  with specific shRNAs could also decrease the levels of phosphorylated PKM2-T454 (Figure 6H). These data suggest that PKM2 is a substrate for CaMKII $\delta$ .

To further verify that CaMKII $\delta$  could directly phosphorylate PKM2, we carried out in vitro phosphorylation assay. Incubation of GST-PKM2 expressed in *Escherichia coli* with CaMKII $\delta$  could significantly lead to the phosphorylation of PKM2-T454, whereas the kinase-dead CaMKII $\delta$ -T287A only resulted in trace level of phosphorylated PKM2-T454 (Figure 6I).

Taken together, these data demonstrated that PKM2 is a bona fide substrate for CaMKII $\delta$ , which phosphorylated it directly at T454.

### Phosphorylated PKM2-T454 Is Essential for the Phosphorylation of PKM2-Y105 and Its Subsequent Role in Pancreatic TIC Properties

The fact that phosphorylated PKM2-Y105 could induce stem-like properties in breast cancer cells<sup>28</sup> prompted us to address whether phosphorylated PKM2-Y105 was also

related to  $\alpha 2\delta 1^+$  pancreatic TICs, and whether there was any relationship between phosphorylated PKM2-T454 and phosphorylated PKM2-Y105. Notably, the levels of phosphorylated PKM2-Y105 were positively correlated with those of phosphorylated PKM2-T454, showing also much higher levels in  $\alpha 2\delta 1^+$  pancreatic TICs and  $\alpha 2\delta 1$ -OE PANC-1 and BxPC-3 cells (Figure 6E). Ectopic expression of CaMKII $\delta$  in PANC-1 cells also dramatically led to the phosphorylation of PKM2-Y105, whereas the kinase-dead construct CaMKII $\delta$ -T287A failed to induce such a phosphorylation (Figure 6F). Treatment of  $\alpha 2\delta 1$ -OE PANC-1 cells with CaMKII inhibitor KN-93, or knockdown of CaMKII $\delta$  with specific shRNAs, could also decrease the levels of phosphorylated PKM2-Y105, which is a similar change to phosphorylated PKM2-T454 did (Figure 6G and H). We then tested whether the phosphorylation of PKM2 at T454 was required for the phosphorylation of PKM2-Y105 by reconstituting the expression of RNAi-resistant wild-type, a phosphodeficient mutant PKM2-T454A, and phosphomimetic mutant PKM2-T454D in  $\alpha 2\delta 1$ -OE PANC-1 cells with endogenous PKM2 knocked down (PKM2-KD) by specific shRNA. Interestingly, the phosphomimetic mutant PKM2-T454D was enough to induce the phosphorylation of PKM2 at Y105, whereas the mutant PKM2-T454A failed to induce such a phosphorylation (Figure 6J), suggesting that the phosphorylation of PKM2-T454 is critical for the phosphorylation of PKM2-Y105.

It was reported that the phosphorylation of PKM2 at Y105 could result in PKM2 homotetramer dissociation into dimers by releasing fructose 1,6-bisphosphate from tetramers, which decreased the PK activity of PKM2, and was linked to translocation of it into nucleus and increased tumorigenicity.<sup>28</sup> Interestingly, we found that most of the phosphomimetic mutant PKM2-T454D proteins formed dimers and translocated into nucleus, which was co-stained by phosphor-PKM2-Y105 antibody, whereas the majority of phosphodeficient mutant PKM2-T454A failed to form dimers and was mainly localized in cytoplasm (Figure 7A and B).

Next, we detected the effects of the phosphorylation of PKM2 on the sphere formation and tumorigenicity abilities

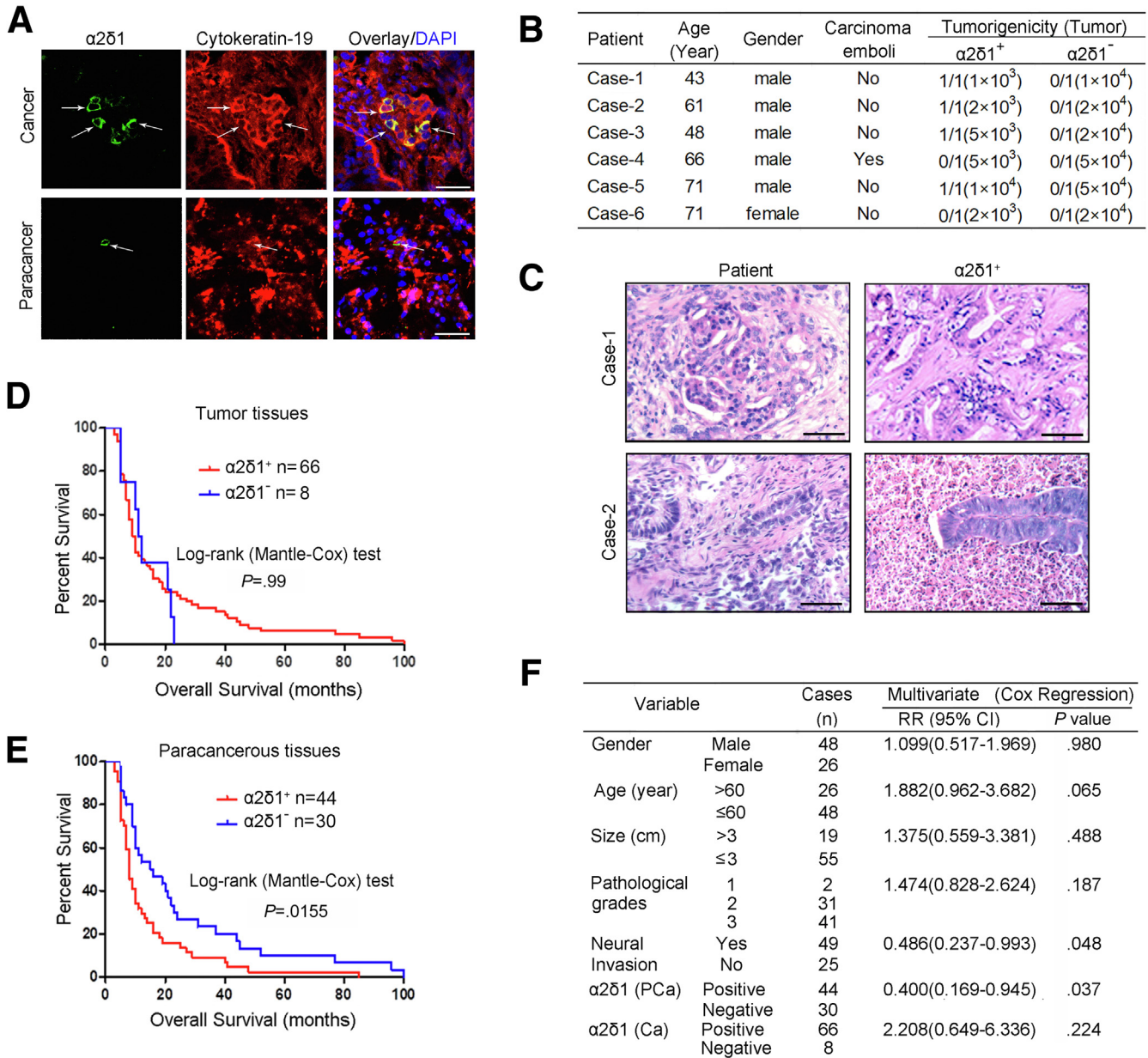


**Figure 3. Clinical significance of  $\alpha 2\delta 1$  expression in PDAC and paracancerous tissues.** (A) Representative images showing results of immunofluorescent staining for  $\alpha 2\delta 1$  with mAb1B50-1 and cytokeratin 19 in cryostat sections of PDAC and paracancerous tissues. Nuclei were stained with DAPI. Scale bars: 50  $\mu\text{m}$ . (B) Tumorigenicity of  $\alpha 2\delta 1^+$  and  $\alpha 2\delta 1^-$  fractions purified directly from freshly resected PDAC tissues. Data are expressed as number of tumors formed/number of sites injected, and the numbers in parentheses represent the numbers of cells injected. (C) Representative images of H&E staining showing histology of tumors formed by  $\alpha 2\delta 1^+$  cells from PDAC tissues, as well as that of original tumor tissues from respective patients. Scale bars: 50  $\mu\text{m}$ . (D and E) Kaplan-Meier curves showing overall survival for PDAC patients divided by  $\alpha 2\delta 1$  staining status in the cancer (D) and paracancerous tissues (E). (F) Multivariate analysis predicts risk factors of poor survival for PDAC patients. Ca, cancer tissue; PCa, paracancerous tissue; RR, relative risk.

of these phosphodeficient and phosphomimetic mutants. Expression of PKM2-T454D or Y105D remarkably led to increased spheroid formation efficiencies and enhanced tumorigenicity, compared with the cells expressing PKM2-WT, whereas expression of PKM2-T454A and PKM2-Y105F did not (Figure 7C-E, Table 4). However, when ectopic expression of PKM2-T454D with an additional Y105F mutation (PKM2-Y105F-T454D), the prompting

effects of PKM2-T454D on the sphere-forming and tumorigenic abilities of PANC-1 cells diminished (Figure 7C-E, Table 4). These data suggested that the phosphorylation of PKM2 at T454 was sufficient to induce stem-like properties of pancreatic TICs, which was dependent on the phosphorylation of PKM2 at Y105 synergistically.

As additional evidence to support the role of  $\alpha 2\delta 1$  in promoting PDAC TIC properties through CaMKII $\delta$ -mediated



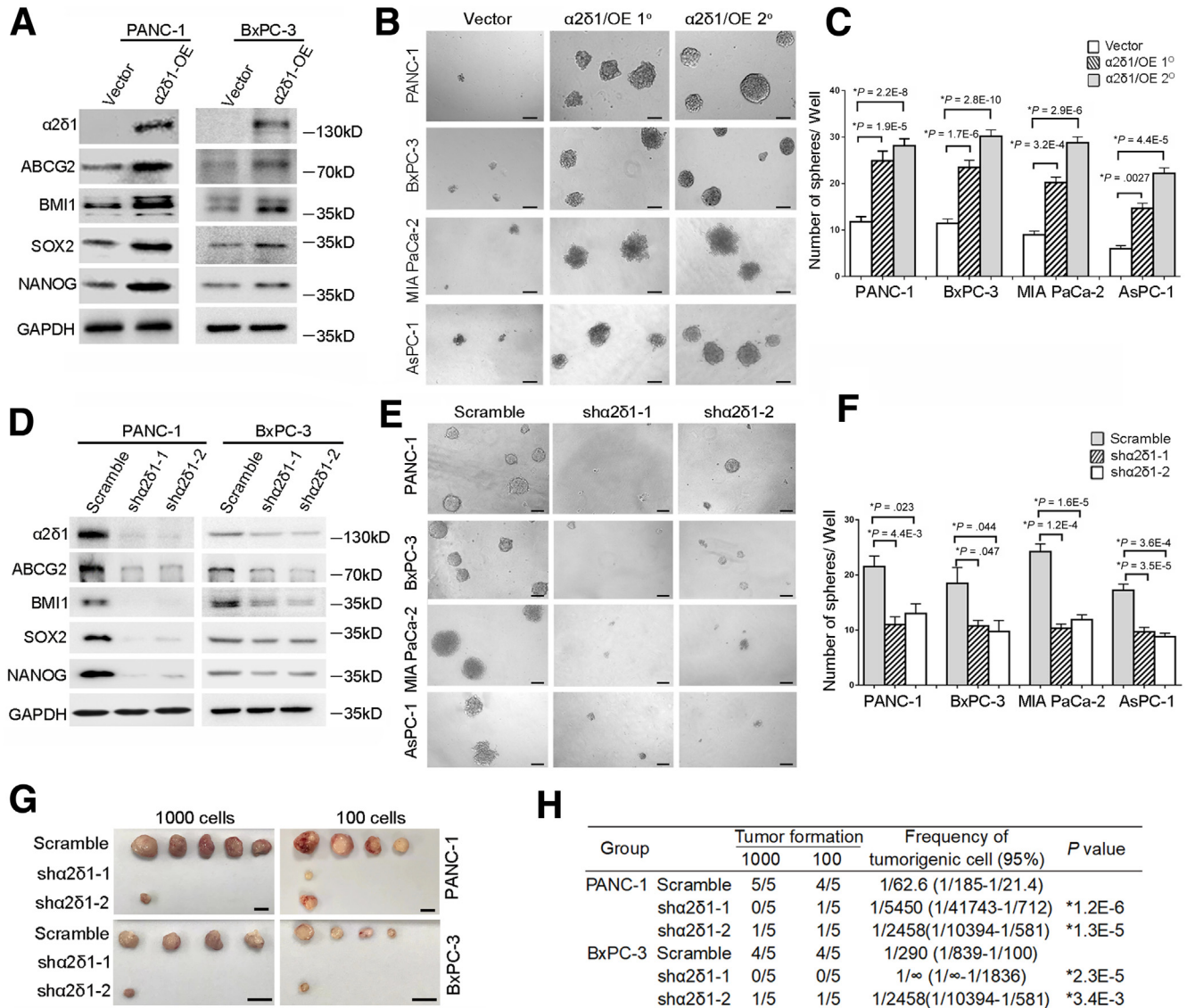


**Figure 4.** Roles of  $\alpha 2\delta 1$  in acquisition and maintenance of stem cell-like properties of PDAC TICs. Western blotting results showing expression of indicated molecules in indicated cell lines overexpressing  $\alpha 2\delta 1$ . (B and C) Phase contrast micrographs (B) and histograms (C) demonstrating primary ( $1^\circ$ ) and serially passaged ( $2^\circ$ ) spheres formed by indicated cells after forced expression of  $\alpha 2\delta 1$ . Scale bars: 100  $\mu\text{m}$ . (D) Expression of indicated molecules in  $\alpha 2\delta 1^+$  fractions sorted from indicated sources after knockdown of  $\alpha 2\delta 1$  by specific shRNAs was detected by Western blotting. (E and F) Representative phase contrast micrographs (E) and histograms (F) showing change of spheroid formation efficiency of sorted  $\alpha 2\delta 1^+$  fractions from indicated sources after  $\alpha 2\delta 1$  knockdown. Scale bars: 100  $\mu\text{m}$ . (G) Photographs demonstrating tumors formed by indicated  $\alpha 2\delta 1^+$  fractions infected with lentiviruses harboring expression cassettes of scramble or  $\alpha 2\delta 1$  shRNAs. Bars = 1 cm. (H) Tumor-initiating cell frequencies of purified  $\alpha 2\delta 1^+$  fractions from indicated sources after  $\alpha 2\delta 1$  shRNA knockdown. Data in C and D represent mean  $\pm$  standard deviation of 3 independent experiments (n = 6). \*Two-tailed Student *t* test.

subsequent phosphorylation of PKM2 at T454 and Y105, the expression of  $\alpha 2\delta 1$  was positively correlated with CaMKII $\delta$ , p-PKM2-Y105, and p-PKM2-T454, and there was a positive correlation between p-PKM2-T454 and p-PKM2-Y105 as demonstrated by immunohistochemical staining in 30 cases of PDAC specimen (Figure 7F-K).

### Blocking $\alpha 2\delta 1$ Reduces TICs and Inhibits the Growth of PDAC in Vivo

The abovementioned results led us to test whether blocking the function of  $\alpha 2\delta 1$  with mAb1B50-1 could have

any therapeutic effects on PDAC by reducing TICs. NOD/SCID mice bearing established xenografts of the cell lines PANC-1 and BxPC-3 were administered intraperitoneally (i.p.) with mAb1B50-1 at 800  $\mu\text{g}$  per mouse alone, gemcitabine (GEM) (60 mg/kg), or combination of both. The treatment with mAb1B50-1 alone could suppress significantly the growth of both the xenografts in NOD/SCID mice, whereas the combinational treatment of mAb1B50-1 with GEM led to superior inhibition of the growth of the tumors to any single regimen by ratios of as many as 78.8% and 75% on PANC-1 and BxPC-3 xenografts, respectively,

lasting for additional periods after termination of the treatments (Figure 8A-F). Notably, there were no significant side effects observed for these treatments because the body weights of the mice remained stable during the treatment period (Figure 8G). The therapeutic effects of

these treatments were further validated in 2 patient-derived xenografts (PDX) (Figure 8H and I). Interestingly, the overall survival of the mice was also improved significantly after combinational therapy in these PDX models (Figure 8J and K).

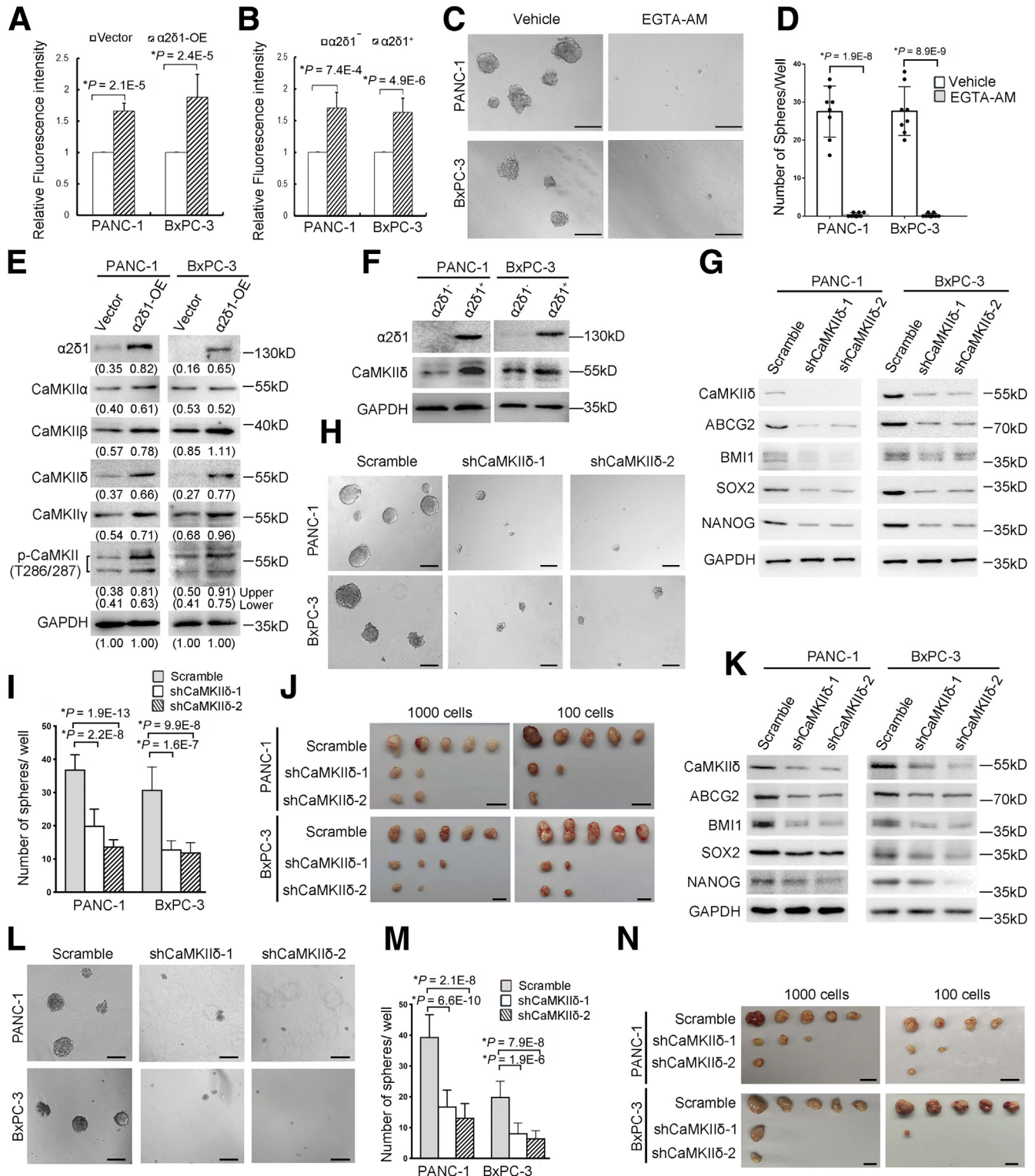


**Table 3.** Tumorigenicity of  $\alpha 2\delta 1$  Overexpression Cells and Sorted  $\alpha 2\delta 1^+$  Subpopulations after CaMKII $\delta$  Knockdown with shRNAs

Group	Tumor formation		Tumorigenic cell frequency (95% CI)	P value
	1000	100		
$\alpha 2\delta 1$ overexpression cells				
PANC-1				
Scramble	5/5	5/5	1 (1/125–1)	
shCaMKII $\delta$ -1	2/5	2/5	1/1061 (1/3128–1/360)	4.7E-6 <sup>a</sup>
shCaMKII $\delta$ -2	2/5	1/5	1/1445 (1/4728–1/442)	1.5E-6 <sup>a</sup>
BxPC-3				
Scramble	5/5	5/5	1 (1/125–1)	
shCaMKII $\delta$ -1	3/5	2/5	1/711 (1/1928–1/262)	3.3E-5 <sup>a</sup>
shCaMKII $\delta$ -2	2/5	2/5	1/1061 (1/3128–1/360)	4.7E-6 <sup>a</sup>
Sorted $\alpha 2\delta 1^+$ subpopulation				
PANC-1				
Scramble	5/5	4/4	1 (1/156–1)	
shCaMKII $\delta$ -1	3/5	2/4	1/689 (1/1894–1/251)	1.6E-4 <sup>a</sup>
shCaMKII $\delta$ -2	1/5	1/4	1/2408 (1/10220–1/567)	1.3E-6 <sup>a</sup>
BxPC-3				
Scramble	5/5	5/5	1 (1/125–1)	
shCaMKII $\delta$ -1	1/5	1/5	1/2458 (1/10394–1/581)	1.6E-7 <sup>a</sup>
shCaMKII $\delta$ -2	1/5	0/5	1/4983 (1/35191–1/706)	2.9E-8 <sup>a</sup>

<sup>a</sup>Compared with respective Scramble group.

To address whether the treatments with mAb1B50-1 could reduce TICs, we first analyzed the TIC proportions in the residues of treated PANC-1 engraftments by flow cytometry. The population of  $\alpha 2\delta 1^+$  TICs decreased upon mAb1B50-1 treatments, especially with the combinational regimen, whereas the proportion of such population enriched by a rate of about 5.5-fold after GEM alone treatment (Figure 8L). Moreover, re-transplantation of 10,000 cells from the residual tumor that received mAb1B50-1 treatment into secondary mice could only initiate the formation of very tiny nodules in 2 of 5 mice, whereas the cells from the control and GEM-treated tumors subsequently generated tumors in almost all the transplanted mice, with GEM-treated cells developing tumors faster and bigger. Notably, the residual tumor cells from the combinational therapy group only formed a negligible nodule in 1 of 5 mice injected (Figure 8M), suggesting that TICs were reduced after mAb1B50-1 treatments.

## Discussion

Here, we found that the  $\alpha 2\delta 1^+$  cells isolated from PDAC cell lines and fresh tissues could generate heterogeneous tumors that histologically recapitulated the primary tumors they derived. These  $\alpha 2\delta 1^+$  cells were commonly shared by CD44<sup>+</sup>, EpCAM<sup>+</sup>, DCLK1<sup>+</sup>, and CD9<sup>+</sup> PDAC cells, previously reported TIC subpopulations of PDAC. Moreover,  $\alpha 2\delta 1$  mediated calcium influx into cells, which subsequently activated CaMKII $\delta$  to enable the acquisition of stem cell-like properties by phosphorylating PKM2. Therefore, we identified  $\alpha 2\delta 1$  as a robust and functionally significant marker for PDAC TICs.

Aberrant expression and/or activation of a particular member of CaMKIIs have been linked to cancer cell proliferation,<sup>31</sup> epithelial-to-mesenchymal transition,<sup>32</sup> invasion and metastasis,<sup>33,34</sup> and their roles in TICs or cancer stem cells are emerging.<sup>35</sup> In the current study, we identified that CaMKII $\delta$  was up-regulated by  $\alpha 2\delta 1$  and served as the major CaMKII that was responsible for  $\alpha 2\delta 1$ -mediated acquisition

**Figure 5.** (See previous page). CaMKII $\delta$  is required for stem cell-like properties promoted by  $\alpha 2\delta 1$ . (A and B) [ $\text{Ca}^{2+}$ ]<sub>i</sub> levels were measured using flow cytometry with  $\text{Ca}^{2+}$  probe Fluo-4/AM in indicated cells overexpressing  $\alpha 2\delta 1$  (A) and FACS-sorted  $\alpha 2\delta 1^+$  and  $\alpha 2\delta 1^-$  fractions from indicated cell lines (B). (C and D) Representative phase contrast micrographs (C) and histograms (D) showing spheroid formation abilities of  $\alpha 2\delta 1^+$  cells from indicated sources after treatment with EGTA-AM at 10  $\mu\text{mol/L}$ . Scale bars: 100  $\mu\text{m}$ . (E and F) Western blotting results showing expression of indicated molecules in indicated cell lines overexpressing  $\alpha 2\delta 1$  (E) and sorted  $\alpha 2\delta 1^+$  and  $\alpha 2\delta 1^-$  fractions from indicated sources (F). (G) Western blot analysis of indicated molecules in  $\alpha 2\delta 1$ -OE cells of indicated sources after knockdown of CaMKII $\delta$  by specific shRNAs. (H and I) Representative phase contrast images (H) and histograms (I) demonstrating spheroid formation abilities of  $\alpha 2\delta 1$ -OE cells from indicated sources after knockdown of CaMKII $\delta$ . Scale bars: 100  $\mu\text{m}$ . (J) Tumorigenicity of indicated cell lines overexpressing  $\alpha 2\delta 1$  infected with lentiviruses harboring shRNA expression cassettes for scramble and CaMKII $\delta$ . Bars = 1 cm. (K) Expression of indicated molecules was analyzed in sorted  $\alpha 2\delta 1^+$  fractions from indicated cell lines after knockdown of CaMKII $\delta$  by specific shRNAs. (L and M) Phase contrast micrographs (L) and histograms (M) showing change of spheroid formation efficiencies in FACS-purified  $\alpha 2\delta 1^+$  fractions upon knockdown of CaMKII $\delta$  by specific shRNAs. Scale bars: 100  $\mu\text{m}$ . (N) Tumorigenicity of  $\alpha 2\delta 1^+$  fractions purified from indicated sources after knockdown of CaMKII $\delta$  by specific shRNAs. Bars = 1 cm. Data in A, B, D, I, and M represent mean  $\pm$  standard deviation of 3 independent experiments. \*Two-tailed Student *t* test.

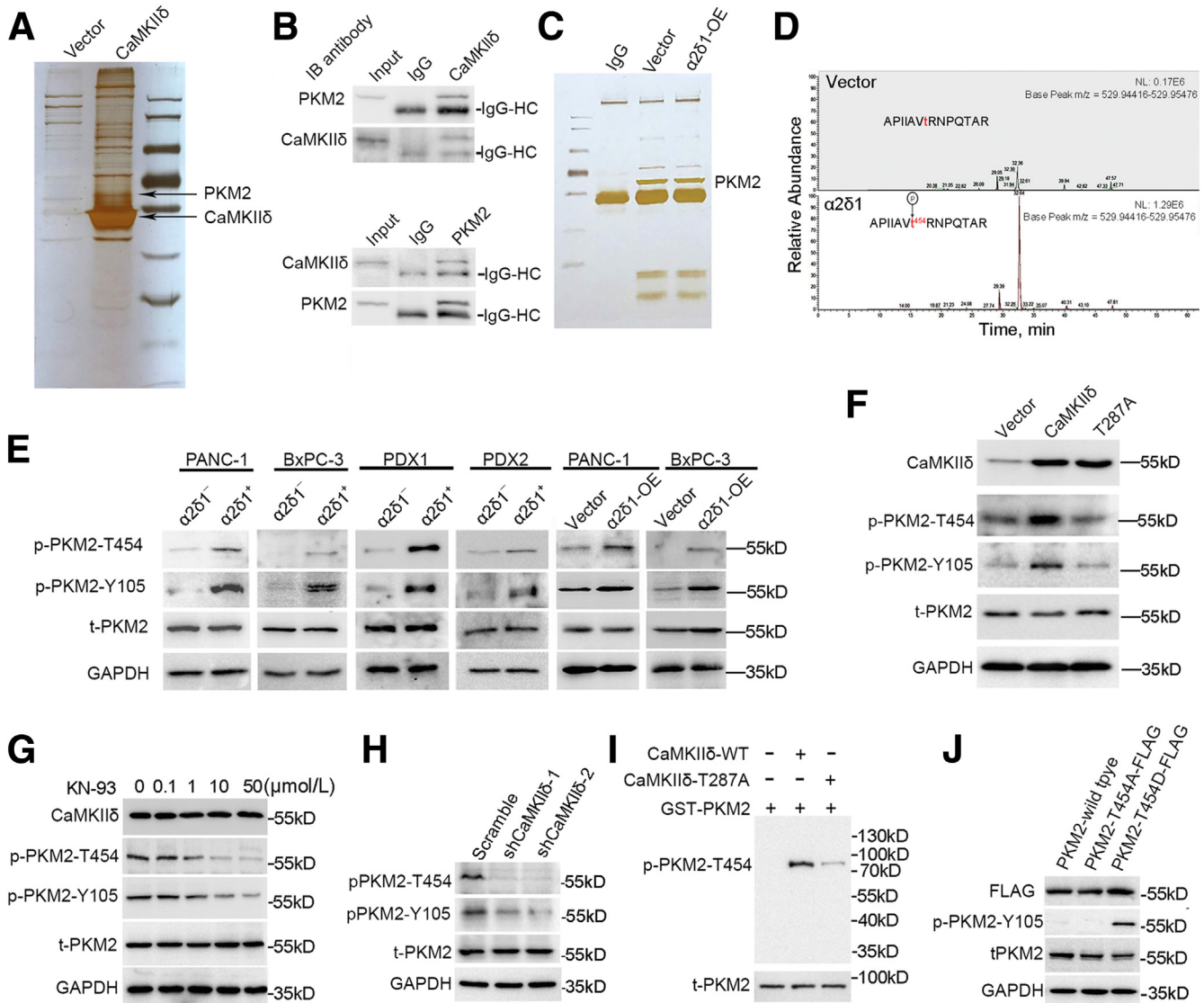


**Figure 6. CaMKII $\delta$  directly phosphorylates PKM2 at T454.** (A) SDS-PAGE analysis of immunoprecipitated products with Flag-resin in PANC-1 cells forced expression of CaMKII $\delta$ -Flag construct. Precipitated products in the cells transfected with vector alone serve as a control. Bands that contained PKM2 and CaMKII $\delta$  as identified by mass spectrum are shown. (B) Western blotting analysis of immunoprecipitated products with indicated antibodies in  $\alpha 2\delta 1$ -OE PANC-1 cells. (C) PKM2 was immunoprecipitated from cell lysates of PANC-1 cells infected with vector alone or  $\alpha 2\delta 1$ -OE lentivirus and was separated by SDS-PAGE for phosphorylation analysis by mass spectrum. (D) Analysis of phosphorylated sites of PKM2 by mass spectrometry in PANC-1 cells overexpressing vector alone or  $\alpha 2\delta 1$ . (E) Western blot analysis with indicated antibodies in sorted  $\alpha 2\delta 1^+$  and  $\alpha 2\delta 1^-$  fractions, as well as the cells overexpressing  $\alpha 2\delta 1$  from indicated sources. (F) PANC-1 cells were transiently transfected with vector, CaMKII $\delta$ , and CaMKII $\delta$ -T287A and were analyzed by Western blotting with indicated antibodies. (G) Western blotting analysis was performed with indicated antibodies in cell lysates of  $\alpha 2\delta 1$ -OE PANC-1 cells treated with KN-93 at indicated concentration for 48 hours. (H) Western blotting analysis with indicated antibodies in cell lysates of  $\alpha 2\delta 1$ -OE PANC-1 cells after knockdown of CaMKII $\delta$  with shRNAs. (I) Western blotting analysis of in vitro phosphorylation assay products with indicated antibodies. Purified GST-PKM2 on glutathione agarose beads were incubated with purified CaMKII $\delta$ -Flag or CaMKII $\delta$ -T287A-Flag in the presence of CaM and ATP. (J) Cell lysates of PKM2-KD PANC-1 cells overexpressing the indicated RNAi-resistant constructs were analyzed by Western blotting with indicated antibodies. IB, immunoblot; t-PKM2, total PKM2.

of TIC properties of PDAC. Although it requires more work to address how CaMKII $\delta$  was up-regulated by  $\alpha 2\delta 1$ , it is possible that calcium influx mediated by  $\alpha 2\delta 1$  will activate the basal level of one or more member(s) of the CaMKII family through Ca<sup>2+</sup>/CaM binding, resulting in activated calcium signaling cascade(s) to up-regulated CaMKII $\delta$ . This

hypothesis was supported by the fact that the phosphorylated CaMKII at Thr286/287 was enhanced after forced expression of  $\alpha 2\delta 1$ . Moreover, PKM2 was demonstrated as a novel substrate for CaMKII $\delta$  involved in such a process. The phosphorylation of PKM2 at T454 mediated by CaMKII $\delta$  led to subsequent phosphorylation of PKM2 at Y105. Because

the phosphorylated PKM2-Y105 was previously reported to have decreased PK activity after the dissociation of PKM2 tetramers into dimers, which was associated with the acquirement of stem-like properties by inducing the

translocation of YAP to activate downstream YAP signaling pathway,<sup>28</sup> we proposed that CaMKII $\delta$  relayed elevated calcium signaling to the transition of the role of PKM2 in PK activity to non-metabolic function in the determination of

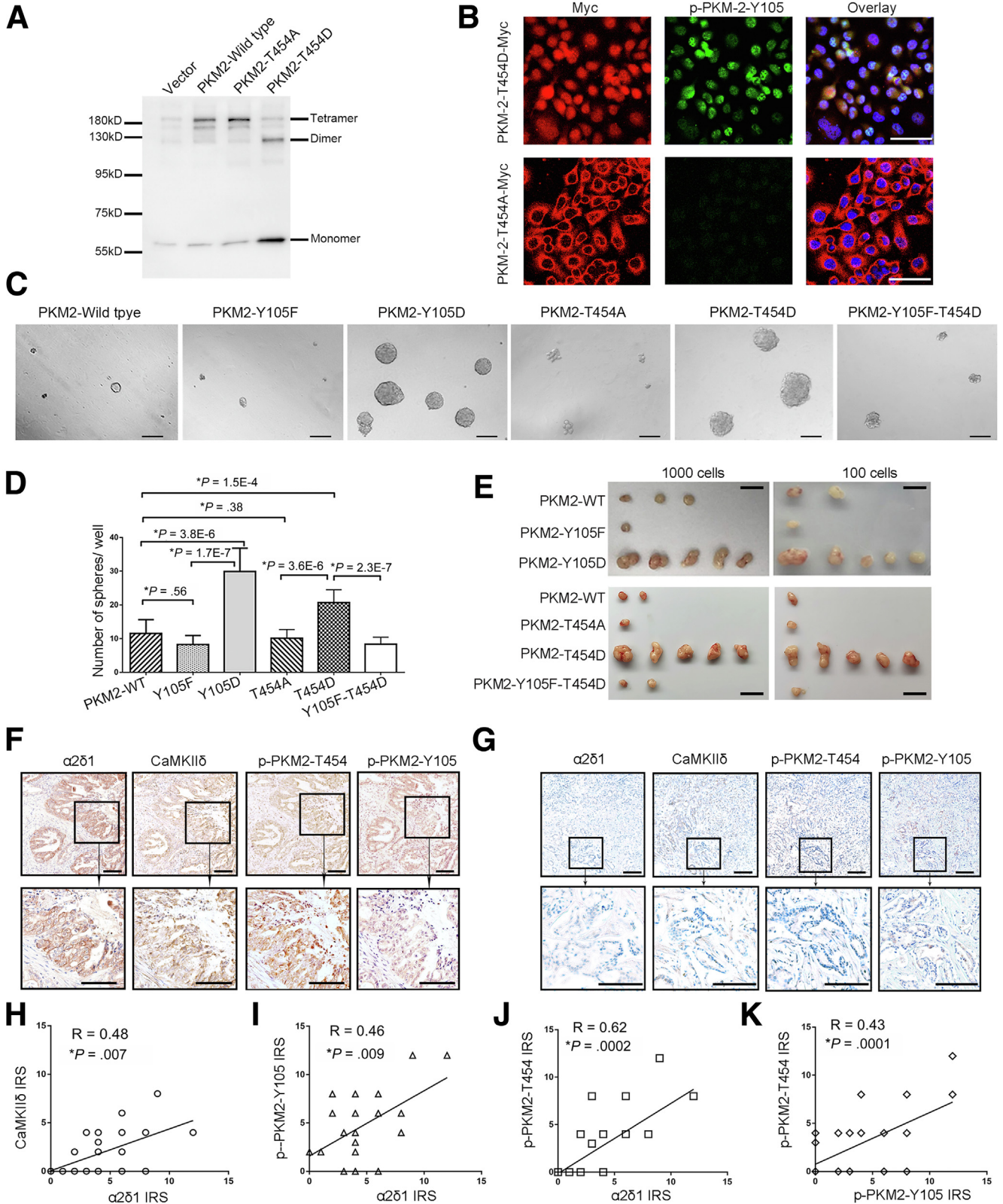


**Table 4.** Tumorigenicity of the PKM2-KD PANC-1 Cells that Ectopically Expressed the Indicated RNAi-Resistant PKM2 Mutants

Group	Tumor formation		Tumorigenic cell frequency (95% CI)	P value
	1000	100		
Set 1 experiment				
PKM2-Wild-type	3/5	2/5	1/711 (1/1928–1/262)	0.122 <sup>a</sup> 3.3E-05 <sup>a</sup>
PKM2-Y105A	1/5	1/5	1/2458 (1/10394–1/581)	
PKM2-Y105D	5/5	5/5	1 (1/125–1)	
Set 2 experiment				
PKM2-Wild-type	2/5	1/5	1/1445 (1/4728–1/442)	0.559 <sup>a</sup> 1.5E-06 <sup>a</sup> 1.0 <sup>a</sup>
PKM2-T454A	1/5	1/5	1/2458 (1/10394–1/581)	
PKM2-T454D	5/5	5/5	1 (1/125–1)	
PKM2-Y105F-T454D	2/5	1/5	1/1445 (1/4728–1/442)	

<sup>a</sup>Compared with the respective PKM2-Wild type group.

cancer stem-like properties of  $\alpha 2\delta 1^+$  PDAC TICs through the phosphorylation of PKM2 at T454 to activate YAP signaling pathway.

The phosphorylation of PKM2 could occur at multiple sites, such as Ser37,<sup>36</sup> Tyr105,<sup>28</sup> and Thr454 as reported here. Each of the phosphorylated PKM2 at Ser37, Tyr105, or Thr454 was able to result in the translocation of PKM2 into nucleus.<sup>28,36,37</sup> Our data supported a sequential phosphorylation mode for PKM2. The phosphorylation occurred first at Thr454 of PKM2 triggered by CaMKII $\delta$ , which possibly increased the accessibility of other kinases to Tyr105, and subsequently led to the phosphorylation at Y105. The phosphorylation of PKM2-T454 was both necessary and sufficient for its phosphorylation at Y105. Hence, the role of phosphorylated PKM2-Y105 in inducing stem-like properties of cancer cells as reported in literature<sup>28</sup> was indeed dependent on the phosphorylation of T454. It would be interesting to determine whether the modifications of PKM2 at other sites such as Ser37 were also affected by T454 phosphorylation.

Here, we demonstrated that the  $\alpha 2\delta 1^+$  cells were also presented in some of the paracancerous tissues of PDAC, and the existence of such a population in the paracancerous tissues was predictive of poor prognosis of PDAC patients. These findings are consistent with our previous work on hepatocellular carcinoma,<sup>22</sup> supporting the hypothesis that  $\alpha 2\delta 1^+$  TICs in paracancerous tissues represent a putative cell-of-origin for the recurrence of respective cancers including PDAC.<sup>38</sup> Further prospective studies using clinical cohorts are warranted to address the prognostic value of the presence of  $\alpha 2\delta 1^+$  TICs in the paracancerous tissues for PDAC patients.

Calcium influx mediated by  $\alpha 2\delta 1$  triggers a plethora of intracellular signaling cascades such as MAPK signaling and NOTCH pathway, which are essential for the self-renewal, survival, drug-resistance, and tumorigenic properties of the TICs of a variety of cancer types; hence targeting  $\alpha 2\delta 1$  with mAb1B50-1 to prevent calcium influx can block these signaling pathways, providing a novel strategy for targeted therapy against TICs of liver and lung origins.<sup>23</sup> Our study here revealed that  $\alpha 2\delta 1$  was also a therapeutic target for PDAC, further indicating that this strategy was also possibly applied to other cancer types.

In conclusion, the results presented here reveal the role of CaMKII $\delta$ , which senses elevated calcium mediated by  $\alpha 2\delta 1$  to transit PKM2 from PK activity to nonmetabolic function through a sequential phosphorylation mode, in the acquisition and subsequent maintenance of the properties of PDAC TICs. Future study is warranted to address whether this calcium signaling pathway is a general mechanism applied to all the other  $\alpha 2\delta 1^+$  TICs from different cancer types. The identification of  $\alpha 2\delta 1$  as a more robust TIC surface marker and therapeutic target for PDAC not only lays the foundation for a better understanding of the nature of TICs, but also provides novel strategies for the prediction of prognosis and targeted therapy against PDAC TICs.

## Materials and Methods

### Cell Lines and Clinical Samples

The pancreatic carcinoma cell lines AsPC-1, MIA PaCa-2, PANC-1, and BxPC-3 were purchased from American Type

**Figure 7.** (See previous page). Effects of phosphorylated PKM2 on stem cell-like properties of PDAC cells. (A) Western blotting analysis with PKM2 antibody to detect PKM2 tetramers or dimers in PKM2-KD PANC-1 cells overexpressing the indicated constructs that are RNAi-resistant. (B) Immunofluorescent staining with indicated antibodies in PANC-1 cells ectopically overexpressing the indicated constructs. Scale bars: 50  $\mu$ m. (C) Representative phase contrast images demonstrating the spheroids formed by PKM2-KD PANC-1 cells overexpressing the indicated RNAi-resistant constructs. Scale bars: 100  $\mu$ m. (D) Histograms showing the spheroid formation efficiencies of the PKM2-KD PANC-1 cells overexpressing the indicated RNAi-resistant constructs. Data represent mean  $\pm$  standard deviation of 3 independent experiments. \*Two-tailed Student *t* test. (E) Tumorigenicity of the PKM2-KD PANC-1 cells overexpressing the indicated RNAi-resistant constructs. Bars = 1 cm. (F and G) Representative immunohistochemical staining images showing high expression (F) and low expression (G) of the indicated molecules in human PDAC samples. Scale bars: 100  $\mu$ m. (H–K) Correlation between the immunoreactive score (IRS) of the immunohistochemical staining of the indicated molecules in human PDAC samples (n = 30).

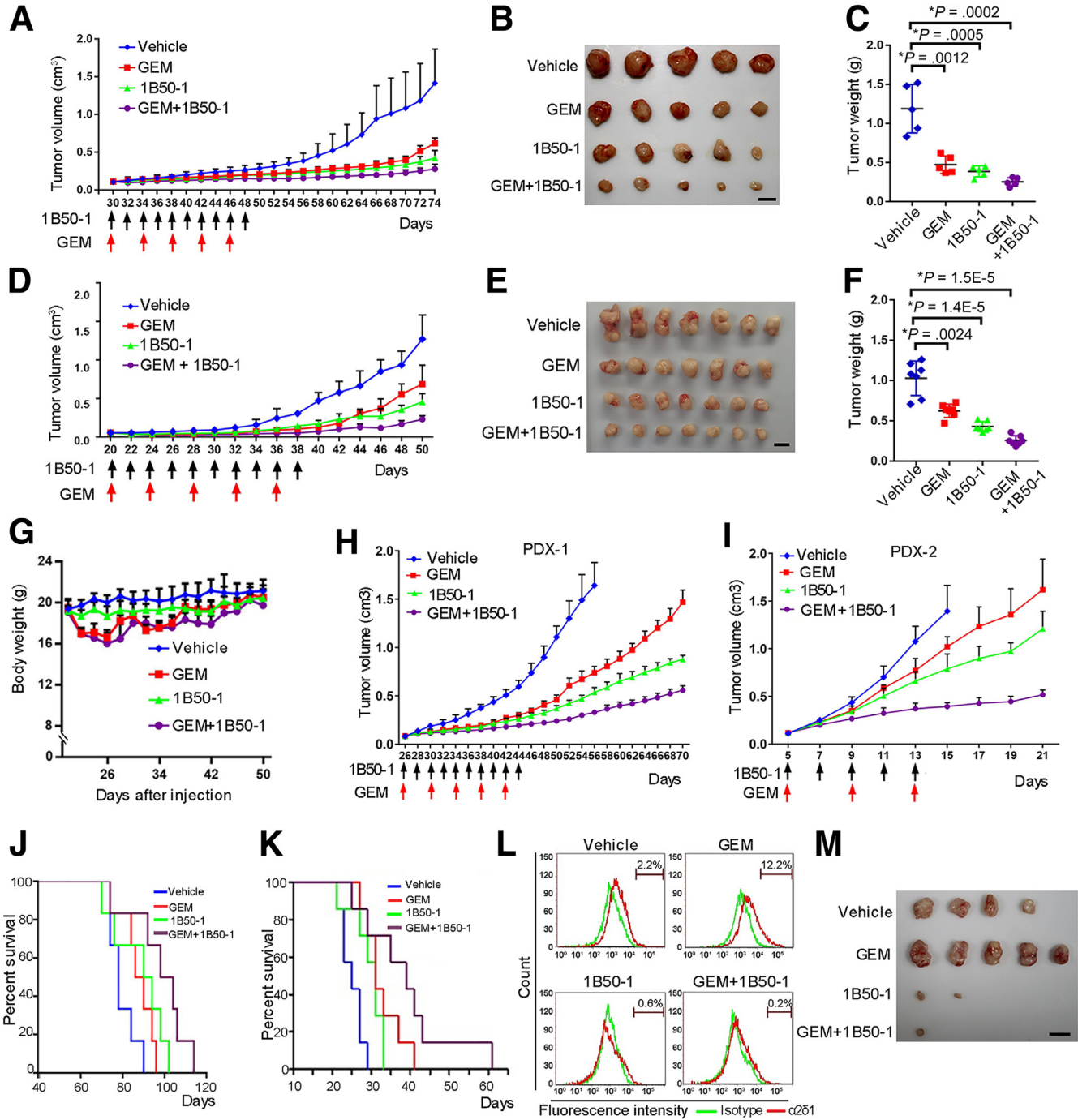


**Figure 8. Therapeutic effects of mAb1B50-1 on PDAC xenografts.** (A–C) Growth curves (A), photograph of dissected tumors (B), and tumor weights (C) of the PANC-1 engraftments treated with mAb1B50-1 (800  $\mu$ g/mice), gemcitabine (GEM) (50 mg/kg), or combination of both after the tumors were visible. (D–F) Growth curves (D), photograph of dissected tumors (E), and tumor weights (F) of BxPC-3 xenografts received the indicated treatments. (G) Body weights of the mice during the treatment period. (H and I) Growth curves showing therapeutic effects of indicated regimens on 2 pancreatic PDX models. (J and K) Kaplan-Meier curves showing the overall survival of PDX-1 (J) and PDX-2 (K) models after the treatments. (L) Flow cytometry analysis of percentage of  $\alpha 2\delta 1^+$  cells in the residual tumors of PANC-1 xenografts after the indicated treatments. (M) Dissected tumors showing the tumor-initiating ability of the PANC-1 engraftment residues after the indicated treatments, which was assayed by re-transplanting  $10^4$  cells per site with Matrigel into NOD/SCID mice. \*Two-tailed Student *t* test. Arrows in A, D, H, and I show the time points that the indicated regimens were administered. Bars = 1 cm.

**Table 5.** Sequences for PCR Primers and shRNA Constructs

Name	Primer	Sequences
PKM2 Wild-type	Forward	5'-CGGGATCCATGTCGAAGCCCCATAGTGAAGC-3'
	Reverse	5'-CCGCTCGAGCGGCACAGGAACAACACGCATG-3'
PKM2 shRNA	Forward	5'-gatccCTGTGGCTCTAGACACTAAActtctgtcagaTTTAGTGTCTAGAGCCACAGtttttG-3'
	Reverse	5'-aattcAAAAACTGTGGCTCTAGACACTAAAtctgacaggaagTTTAGTGTCTAGAGCCACAGg-3'
PKM2-Y105F	Forward	5'-CCTCTTCCGGCCCGTTGCTGTGG-3'
	Reverse	5'-GCCGGAAGAGGATGGGGTCAGAAGC-3'
PKM2-Y105D	Forward	5'-TCCTCGACCGGCCCGTTGCTGTG-3'
	Reverse	5'-CCGGTCGAGGATGGGGTCAGAAGC-3'
PKM2-T454A	Forward	5'-CGGGATCCATGTCGAAGCCCCATAGTGAAG-3'
	Reverse	5'-CGAGCTGTCTGGGGATTCCGGGCCACAGCAATGAT-3'
PKM2-T454D	Forward	5'-ATCATTGCTGTGGACCGGAATCCCAGACAGCTCG-3'
	Reverse	5'-CGAGCTGTCTGGGGATTCCGGTCCACAGCAATGAT-3'
CaMKII $\delta$ Wild-type	Forward	5'-CGGGATCCATGGCTTCGACCACAACCTGCA-3'
	Reverse	5'-CCGCTCGAGGATGTTTTGCCACAAGAGGTG-3'
CaMKII $\delta$ shRNA1	Forward	5'-gatccGATCAAGGCTGGAGCTTATcttctgtcagaATAAGCTCCAGCCTTGATCtttttG-3'
	Reverse	5'-aattcaaaaaGATCAAGGCTGGAGCTTATtctgacaggaagATAAGCTCCAGCCTTGATCg-3'
CaMKII $\delta$ shRNA2	Forward	5'-gatccGGTGAGAAGATGTATGAAActtctgtcagaTTTCATACATCTTCTCACCTtttttG-3'
	Reverse	5'-aattcaaaaaGGTGAGAAGATGTATGAAAtctgacaggaagTTTCATACATCTTCTCACCTg-3'
CaMKII $\delta$ T287A	Forward	5'-CACAGACAGGAGGCTGTAGACTGCTTGAAGAAATT-3'
	Reverse	5'-AATTTCTTCAAGCAGTCTACAGCCTCCTGTCTGTG-3'
Scrambled shRNA	Forward	5'-gatccGCGAGAAGCGCGATCACATGTTCAAGAGACATGTGATCGCGCTTCTCGtttttG-3'
	Reverse	5'-aattcaaaaaACGAGAAGCGATCACATGTCTTTGAACATGTGATCGCGCTTCTCGg-3'

Culture Collection (Manassas, VA) and were cultured in RPMI 1640 medium or Dulbecco modified Eagle medium as suggested by the vendor, supplemented with 10% fetal bovine serum, 100 U/mL penicillin, and 100  $\mu$ g/mL streptomycin (Thermo Fisher Scientific, Waltham, MA). Normal human pancreatic duct epithelial cell line HPDE6-C7 was obtained from Kerafast Inc (Boston, MA) and cultured in Keratinocyte Serum Free Medium (Thermo Fisher Scientific) supplemented with 50  $\mu$ g/mL bovine pituitary extract (Thermo Fisher Scientific) and 5 ng/mL epidermal growth factor (Thermo Fisher Scientific). All cell lines were authenticated using short tandem repeat DNA profiling and were cleared off mycoplasma contamination. All cell lines were maintained in an atmosphere of 5% CO<sub>2</sub> at 37°C.

Primary PDAC specimens and paracancerous tissues were obtained from patients who underwent duodenopancreatectomy or pancreatectomy in Peking University Third Hospital with written informed consent. The acquisition and use of these tissues were approved by the Ethics Committee of Peking University Third Hospital (no. G-2014005), and the study was compliant with all relevant ethical regulations regarding research involving human participants. The PDX were established by transplanting mechanically minced PDAC specimens immediately after surgery into NOD/SCID mice (NOD.CB17-*Prkdc*<sup>scid</sup>; Vital River Laboratories, Beijing, China).

### Vector Construction and Lentivirus Packaging

The construction of  $\alpha$ 2 $\delta$ 1 overexpression and shRNA knockdown lentivirus vectors was described in our previous article.<sup>22</sup> The open reading frames of wild-type *CaMK2D* and *PKM2* were polymerase chain reaction amplified from

cDNAs that were reverse-transcribed from total RNAs extracted from the hepatocellular carcinoma cell line Hep-12<sup>39</sup> and were subcloned into pLenti6 vector (Thermo Fisher Scientific) using standard DNA recombinant technique. For all the mutant constructs, respective point mutations were introduced using overlapped polymerase chain reaction with primers harboring the mutations and were cloned into pLenti6 vector. The shRNA-resistant wild-type and mutant *PKM2* constructs were further made by replacing the shRNA targeting sequence with synonymous codons. For the *CaMK2D* and *PKM2* shRNA constructs, synthetic target oligos were cloned into PSIH-H1-Puro vectors. All the primers used are listed in Table 5, and the constructs were validated by sequencing. Lentiviral particles were produced in 293FT cells as described previously.

### Lentivirus Infection

Adherent cells were incubated with lentivirus for overnight, followed by adding selection antibiotics 48 hours later. Surviving cells were expanded for subsequent experiments. For shRNA knockdown assay, FACS-sorted  $\alpha$ 2 $\delta$ 1<sup>+</sup> TICs were incubated with lentivirus for 4 hours at 37°C by spinning slowly in an incubator and were cultured in serum-free medium for additional 72 hours for Western blot assay or were proceeded directly for spheroid formation assay or tumorigenicity assay.

### Living Cell Immunofluorescent Staining and Flow Cytometry

The preparation of single cell suspension, immunofluorescent staining, and flow cytometry was done essentially the same as previously described.<sup>22</sup> In brief, single-cell



**Table 6.** Patient Information for the Pancreatic Carcinoma PDX Models

Variable	PDX1	PDX2
Gender	Male	Male
Age/year	43	61
Pathologic type	Pancreatic ductal adenocarcinoma	Pancreatic ductal adenocarcinoma
Tumor size	5.5 cm	1.2 cm
Pathologic grades	2	3
Lymphatic metastasis	Yes	No
Neural invasion	Yes	Yes
Intravascular carcinoma emboli	Yes	Yes
Choledochus infiltration	Yes	Yes

suspensions from PDAC cell lines, tumor tissues were incubated with the antibodies including mAb1B50-1 against  $\alpha 2\delta 1$  and DCLK1 (Abcam, Cambridge, MA), which were conjugated with fluorescein isothiocyanate or phycoerythrin-cyanin 5 using BD Lightning conjugation kits (Expedeon Ltd, Cambridge, UK), as well as CD44-PE (Miltenyi Biotec, Auburn, CA), EpCAM-FITC (R&D Systems, Minneapolis, MN), and CD9-APC (Thermo Fisher Scientific), followed by washing with phosphate-buffered saline 3 times. After being filtered through a 40- $\mu$ m nylon mesh, the single-cell suspensions were gated, analyzed, or sorted using a FACS Aria II flow cytometer (Becton Dickinson, San Jose, CA). The respective isotype controls were used as references, and data were processed using FlowJo VX software.

### Intracellular Calcium Measurement

Intracellular calcium levels were measured using the Fluo-4/AM probe (Thermo Fisher Scientific) following the published protocol.<sup>22</sup> Labeled cells were analyzed using a FACSCalibur flow cytometer (Becton Dickinson).

### Immunofluorescent and Immunohistochemical Staining

For cultured cell immunofluorescent staining, cells were fixed with 4% paraformaldehyde at room temperature for 10 minutes, permeabilized with 0.5% Triton X-100, and were incubated with primary antibody and secondary antibody as previously described.<sup>40</sup> The immunofluorescent staining of frozen tissues was performed following the protocol described in literature.<sup>22</sup> For immunohistochemical staining, formalin-fixed, paraffin-embedded PDAC specimen sections were deparaffinized and rehydrated, followed by heating for antigen retrieval for 15 minutes in 10 mmol/L citrate (pH 6.0) according to standard protocol. Sections were then incubated with primary antibody at 4°C overnight. Diaminobenzidine staining was performed using DAB detection Kit (polymer) (Beijing Zhongshan Goldenbridge Biotechnology Co, Ltd, Beijing, China) according to the vendor's instructions, followed by hematoxylin counterstaining. The information of the primary antibodies was listed in Table 6. The immunohistochemistry staining was quantified using the immunoreactive score (IRS) (system in a double-blind manner, giving a score range of 0–12 by multiplication of the positive cell proportion score (0 = 0%, 1 = 1%–10%, 2 = 11%–50%, 3 = 51%–80%, and 4 = 81%–100% stained cells) and the staining intensity score (0 = negative, 1 = weak, 2 = moderate, and 3 = strong).

**Table 7.** Information for Antibodies

Name	Vendor	Cat. no.	Species	Dilution
ABCG2	Epitomics	3765-1	Rabbit monoclonal IgG	WB: 1:2000
Nanog	Abcam	ab109250	Rabbit monoclonal IgG	WB: 1:2000
SOX2	Abcam	ab97959	Rabbit monoclonal IgG	WB: 1:2000
BMI1	Abcam	Ab126783	Rabbit monoclonal IgG	WB: 1:5000
FLAG	Origene	TA50011	Mouse monoclonal IgG	WB: 1:5000
$\alpha 2\delta 1$	Abcam	ab2864	Mouse monoclonal IgG	WB: 1:2000
$\alpha 2\delta 1$	Novus	Nb120-2864	Mouse monoclonal IgG	WB: 1:2000
CaMKII $\alpha$	Cell Signaling	3357S	Rabbit polyclonal IgG	WB: 1:2000
CaMKII $\beta$	Invitrogen	13-9800	Mouse monoclonal IgG	WB: 1:2000
CaMKII $\delta$	Santa Cruz	SC-100362	Mouse monoclonal IgG	WB: 1:200; IP: 1:20
CaMKII $\gamma$	Sigma-Aldrich	SAB1400039	Rabbit polyclonal IgG	WB: 1:2000
p-PKM2(Y105)	Cell Signaling	3827S	Rabbit monoclonal IgG	WB: 1:2000
PKM2	Cell Signaling	4053S	Rabbit monoclonal IgG	WB: 1:2000
GAPDH	Bioworld	BS606030	Rabbit polyclonal IgG	WB: 1:20000
PKM2	Abcam	AB131021	Rabbit monoclonal IgG	IP: 1:20
CD44-PE	Miltenyi	130-113-335	Mouse monoclonal IgG	IF: 1:50
EpCAM-FITC	R&D Systems	FAB9601F	Mouse monoclonal IgG	IF: 1:50
DCLK1	Abcam	Ab37994	Rabbit polyclonal IgG	IF: 1:30

### Sphere Formation Assay

Sphere formation assay was performed in ultralow attachment 96-well plates (Corning Incorporated Life Sciences, Acton, MA) by plating 100 cells per well in DMEM/F12 medium supplemented with B27 (Invitrogen, Waltham, MA), 20 ng/mL EGF, 10 ng/mL HGF (Peprotech, Rocky Hill, NJ), 20 ng/mL bFGF (Invitrogen), and 1% methylcellulose (Sigma-Aldrich, St Louis, MO). After cultivation in 5% CO<sub>2</sub> incubator for 2–3 weeks, the spheres with diameter  $\geq 100 \mu\text{m}$  were counted under an Axio Observer A1 inverted microscope (Carl Zeiss Microscopy GmbH, Jena, Germany).

### Tumorigenicity Assay

Female 4- to 6-week-old NOD/SCID mice (Beijing Vital River Laboratory Animal Technology Co, Ltd, Beijing, China) were used in this study following the National Institutes of Health Guide for the Care and Use of Laboratory Animals with protocols approved by the Peking University Cancer Hospital Animal Care and Use Committee. For the tumorigenic potential assay, cells suspended in 100  $\mu\text{L}$  of 1:1 mixture of plain RPMI 1640 medium and Matrigel (BD Biosciences, Bedford, MA) were transplanted s.c. into the back of mice. Tumor formation was monitored weekly, and the tumorigenic cell frequency was determined on the basis of extreme limiting dilution analysis using a web tool at <http://bioinf.wehi.edu.au/software/elda/>.<sup>41</sup> For the therapeutic assay, both PDAC cell line-derived xenografts and PDX (Table 7) were established by transplanting tumor cells/tissues s.c. into the backs of mice. When all the tumors reached palpable size, the mice were randomly separated into 4 groups and were administered i.p. with control vehicle, anti- $\alpha 2\delta 1$  mAb1B50-1 (800  $\mu\text{g}/\text{mice}$ ), GEM (50 mg/kg), and the combination of mAb1B50-1 with GEM for each respective group. The tumors were measured every other day with calipers, and individual tumor volumes ( $V$ ) were determined using the formula:  $V = \text{length} \times \text{width}^2 \times 0.5$ .

### Western Blot

Cells were homogenized in radioimmunoprecipitation assay buffer (50 mmol/L Tris pH 7.4, 150 mmol/L NaCl, 1% NP-40, 0.25% sodium deoxycholate, 0.1% sodium dodecyl sulfate) supplemented with 1 mmol/L phenylmethylsulfonyl fluoride, phosphatase inhibitor cocktail, and Complete Mini protease inhibitor cocktail (Roche, Mannheim, Germany). Equal amounts of proteins were electrophoresed on 10% or 12% sodium dodecyl sulfate-polyacrylamide gel electrophoresis (SDS-PAGE) and were transferred to Immobilon-P PVDF membrane (0.45  $\mu\text{m}$  pore size; Millipore, Billerica, MA). The membranes were blocked with 5% non-fat milk and incubated with primary and secondary antibodies following the protocol described previously.<sup>22</sup> The polyclonal rabbit antibody specifically recognizing phosphorylated PKM2 at Thr454 (p-PKM2-T454) was produced by immunizing rabbits with phosphorylated peptides C-RAPIIAVT(p)RNPQTAR (Huiou Biotech Inc, Shanghai, China). The information on other antibodies used is provided in Table 6. The immuno-complexes were detected using Immobilon Western Chemiluminescent

HRP substrate (Millipore), and the signals were captured with MiniChemi 610 Chemiluminescent Imaging and Analysis System (Beijing Sage Creation Science Co, Ltd., Beijing, China).

### Immunoprecipitation Assay

Cells were extracted with ice-cold CellLytic M lysis buffer (Sigma-Aldrich) plus phosphatase inhibitor cocktail and protease inhibitor cocktail on ice, followed by sonication. Cell extracts were then clarified by centrifugation at 12,000 rpm for 5 minutes, and the supernatants were subjected to immunoprecipitation with mouse anti-CaMKII $\delta$  monoclonal and rabbit anti-PKM2 polyclonal antibodies at 4°C overnight, followed by additional incubation with Protein A/G PLUS-Agarose beads (GE Healthcare, Uppsala, Sweden) for an additional 3 hours. After washing with ice-cold lysis buffer 3 times, proteins binding to the beads were eluted with 1 $\times$  sodium dodecyl sulfate loading buffer. For the Flag-tagged proteins, cell extracts were incubated with anti-Flag M2 affinity gel (A2220; Sigma-Aldrich) overnight at 4°C, and the precipitated proteins were eluted following the anti-Flag M2 gel vendor's recommendation.

### Mass Spectrometry Analysis

The immunoprecipitation products were detected on SDS-PAGE using Pierce Silver Stain for MS kit (Thermo Fisher Scientific). The bands of target proteins were sliced and digested with sequencing grade trypsin in 50 mmol/L NH<sub>4</sub>HCO<sub>3</sub> overnight at 37°C, followed by nano-liquid chromatography with tandem mass spectrometry analysis on an LTQ-velos mass spectrometer interfaced with an EASY nano-LC system (Thermo Fisher Scientific). The liquid chromatography with tandem mass spectrometry data were searched against the human sequence library in the Uniprot protein sequence database using SEQUEST HT algorithm in the Proteome Discoverer 1.4 software package (Thermo Fisher Scientific). The probability of phosphosite localization was calculated using the phosphoRS 3.0 software implemented into the Proteome Discoverer.

### In Vitro Phosphorylation Assay

Flag-tagged CaMKII $\delta$  and CaMKII $\delta$ -T287A mutant were purified from FreeStyle 293 cells (Invitrogen) transiently transfected with respective expression constructs using anti-Flag M2 affinity gel. The fusion protein glutathione S-transferase-PKM2 was expressed in *E coli* Rosetta (DE3) and was purified using glutathione-agarose 4B (GE Healthcare, Uppsala, Sweden) following standard protocol. For the in vitro PKM2 phosphorylation assay, purified wild-type CaMKII $\delta$  or mutant CaMKII $\delta$ -T287A protein was pre-incubated in a reaction mixture containing 35 mmol/L HEPES, pH 8.0, 10 mmol/L MgCl<sub>2</sub>, 0.5  $\mu\text{mol}/\text{L}$  CaM (Prospect, Rehovot, Israel), 5  $\mu\text{mol}/\text{L}$  adenosine triphosphate, and 1 mmol/L CaCl<sub>2</sub> at 30°C for 10 minutes, followed by the addition of glutathione Sepharose 4B beads that bound glutathione S-transferase-PKM2 and further incubation for 2 hours. Glutathione S-transferase-PKM2 were eluted using 2 $\times$  SDS-PAGE loading buffer. The phosphorylation of PKM2

was detected by Western blotting using p-PKM2-T454 antibody.

### Detection of PKM2 Oligomerization

Cultured cells were collected, washed with phosphate-buffered saline, and resuspended in CHAPS buffer (20 mmol/L HEPES-KOH, pH 7.5, 5 mmol/L MgCl<sub>2</sub>, 0.5 mmol/L EGTA, 0.1 mmol/L phenylmethylsulfonyl fluoride) containing 4 mmol/L disuccinimidyl suberate (Thermo Fisher Scientific) at room temperature for 30 minutes to crosslink proteins. After the samples were centrifuged at 5000g for 8 minutes at 4°C, cell pellets were lysed with Tris-free radioimmunoprecipitation assay buffer (50 mmol/L HEPES, pH 7.4, 150 mmol/L NaCl, 1 mmol/L EDTA, 1% NP-40, 0.1% SDS) supplemented with proteinase inhibitor cocktail and phosphatase inhibitors on ice for 30 minutes, followed by sonication. The supernatants were subjected to SDS-PAGE and Western blot analysis.<sup>28,42</sup>

### Statistical Analysis

The data were analyzed using GraphPad Prism software (San Diego, CA). The significance of differences was determined with a double-sided Student *t* test unless otherwise specified. A *P* value  $\leq .05$  was considered statistically significant.

### References

- Ryan DP, Hong TS, Bardeesy N. Pancreatic adenocarcinoma. *N Engl J Med* 2014;371:1039–1049.
- Siegel RL, Miller KD, Fuchs HE, Jemal A. Cancer statistics, 2021. *CA Cancer J Clin* 2021;71:7–33.
- Crawford HC, Pasca di Magliano M, Banerjee S. Signaling networks that control cellular plasticity in pancreatic tumorigenesis, progression, and metastasis. *Gastroenterology* 2019;156:2073–2084.
- Clara JA, Monge C, Yang Y, Takebe N. Targeting signalling pathways and the immune microenvironment of cancer stem cells: a clinical update. *Nat Rev Clin Oncol* 2020;17:204–232.
- Visvader JE, Lindeman GJ. Cancer stem cells: current status and evolving complexities. *Cell Stem Cell* 2012;10:717–728.
- Wang VM, Ferreira RMM, Almagro J, Evan T, Legrave N, Zaw Thin M, Frith D, Carvalho J, Barry DJ, Snijders AP, Herbert E, Nye EL, MacRae JI, Behrens A. CD9 identifies pancreatic cancer stem cells and modulates glutamine metabolism to fuel tumour growth. *Nat Cell Biol* 2019;21:1425–1435.
- Hermann PC, Huber SL, Herrler T, Aicher A, Ellwart JW, Guba M, Bruns CJ, Heeschen C. Distinct populations of cancer stem cells determine tumor growth and metastatic activity in human pancreatic cancer. *Cell Stem Cell* 2007;1:313–323.
- Gzil A, Zarebska I, Bursiewicz W, Antosik P, Grzanka D, Szyberg L. Markers of pancreatic cancer stem cells and their clinical and therapeutic implications. *Mol Biol Rep* 2019;46:6629–6645.
- Campiglio M, Flucher BE. The role of auxiliary subunits for the functional diversity of voltage-gated calcium channels. *J Cell Physiol* 2015;230:2019–2031.
- Clapham DE. Calcium signaling. *Cell* 2007;131:1047–1058.
- Smedler E, Uhlen P. Frequency decoding of calcium oscillations. *Biochim Biophys Acta* 2014;1840:964–969.
- Brzozowski JS, Skelding KA. The multi-functional calcium/calmodulin stimulated protein kinase (CaMK) family: emerging targets for anti-cancer therapeutic intervention. *Pharmaceuticals (Basel)* 2019;12:8.
- Bayer KU, Schulman H. CaM kinase: still inspiring at 40. *Neuron* 2019;103:380–394.
- Yang E, Schulman H. Structural examination of autoregulation of multifunctional calcium/calmodulin-dependent protein kinase II. *J Biol Chem* 1999;274:26199–26208.
- Rosenberg OS, Deindl S, Sung R-J, Nairn AC, Kuriyan J. Structure of the autoinhibited kinase domain of CaMKII and SAXS analysis of the holoenzyme. *Cell* 2005;123:849–860.
- Roderick HL, Cook SJ. Ca<sup>2+</sup> signalling checkpoints in cancer: remodelling Ca<sup>2+</sup> for cancer cell proliferation and survival. *Nat Rev Cancer* 2008;8:361–375.
- Monteith GR, Prevarskaya N, Roberts-Thomson SJ. The calcium–cancer signalling nexus. *Nat Rev Cancer* 2017;17:373–380.
- O'Reilly D, Buchanan P. Calcium channels and cancer stem cells. *Cell Calcium* 2019;81:21–28.
- Forostyak O, Forostyak S, Kortus S, Sykova E, Verkhatsky A, Dayanithi G. Physiology of Ca<sup>2+</sup> signalling in stem cells of different origins and differentiation stages. *Cell Calcium* 2016;59:57–66.
- Sun C, Shui B, Zhao W, Liu H, Li W, Lee JC, Doran R, Lee FK, Sun T, Shen QS, Wang X, Reining S, Kotlikoff MI, Zhang Z, Cheng H. Central role of IP3R2-mediated Ca<sup>2+</sup> oscillation in self-renewal of liver cancer stem cells elucidated by high-signal ER sensor. *Cell Death Dis* 2019;10:396.
- Han H, Du Y, Zhao W, Li S, Chen D, Zhang J, Liu J, Suo Z, Bian X, Xing B, Zhang Z. PBX3 is targeted by multiple miRNAs and is essential for liver tumour-initiating cells. *Nat Commun* 2015;6:8271.
- Zhao W, Wang L, Han H, Jin K, Lin N, Guo T, Chen Y, Cheng H, Lu F, Fang W, Wang Y, Xing B, Zhang Z. 1B50-1, a mAb raised against recurrent tumor cells, targets liver tumor-initiating cells by binding to the calcium channel  $\alpha 2\delta 1$  subunit. *Cancer Cell* 2013;23:541–556.
- Ma Y, Yang X, Zhao W, Yang Y, Zhang Z. Calcium channel  $\alpha 2\delta 1$  subunit is a functional marker and therapeutic target for tumor-initiating cells in non-small cell lung cancer. *Cell Death Dis* 2021;12:257.
- Zhang Z, Zhao W, Lin X, Gao J, Zhang Z, Shen L. Voltage-dependent calcium channel  $\alpha 2\delta 1$  subunit is a specific candidate marker for identifying gastric cancer stem cells. *Cancer Manag Res* 2019;11:4707–4718.
- Mazurek S. Pyruvate kinase type M2: a key regulator of the metabolic budget system in tumor cells. *Int J Biochem Cell Biol* 2011;43:969–980.

26. Yang W, Xia Y, Hawke D, Li X, Liang J, Xing D, Aldape K, Hunter T, Alfred Yung WK, Lu Z. PKM2 phosphorylates histone H3 and promotes gene transcription and tumorigenesis. *Cell* 2012;150:685–696.
27. Yang W, Xia Y, Ji H, Zheng Y, Liang J, Huang W, Gao X, Aldape K, Lu Z. Nuclear PKM2 regulates beta-catenin transactivation upon EGFR activation. *Nature* 2011;480:118–122.
28. Zhou Z, Li M, Zhang L, Zhao H, Şahin Ö, Chen J, Zhao JJ, Songyang Z, Yu D. Oncogenic kinase-induced PKM2 tyrosine 105 phosphorylation converts non-oncogenic PKM2 to a tumor promoter and induces cancer stem-like cells. *Cancer Res* 2018;78:2248–2261.
29. Luo W, Hu H, Chang R, Zhong J, Knabel M, O’Meally R, Cole RN, Pandey A, Semenza GL. Pyruvate kinase M2 is a PHD3-stimulated coactivator for hypoxia-inducible factor 1. *Cell* 2011;145:732–744.
30. Lobo NA, Shimono Y, Qian D, Clarke MF. The biology of cancer stem cells. *Annu Rev Cell Dev Biol* 2007;23:675–699.
31. Si J, Collins SJ. Activated Ca<sup>2+</sup>/calmodulin-dependent protein kinase II $\gamma$  is a critical regulator of myeloid leukemia cell proliferation. *Cancer Res* 2008;68:3733–3742.
32. Li N, Jiang P, Du W, Wu Z, Li C, Qiao M, Yang X, Wu M. Siva1 suppresses epithelial-mesenchymal transition and metastasis of tumor cells by inhibiting stathmin and stabilizing microtubules. *Proc Natl Acad Sci USA* 2011;108:12851–12856.
33. Daft PG, Yuan K, Warram JM, Klein MJ, Siegal GP, Zayzafoon M. Alpha-CaMKII plays a critical role in determining the aggressive behavior of human osteosarcoma. *Mol Cancer Res* 2013;11:349–359.
34. Cuddapah VA, Sontheimer H. Molecular interaction and functional regulation of CIC-3 by Ca<sup>2+</sup>/calmodulin-dependent protein kinase II (CaMKII) in human malignant glioma. *J Biol Chem* 2010;285:11188–11196.
35. Terrie E, Coronas V, Constantin B. Role of the calcium toolkit in cancer stem cells. *Cell Calcium* 2019;80:141–151.
36. Yang W, Zheng Y, Xia Y, Ji H, Chen X, Guo F, Lyssiotis CA, Aldape K, Cantley LC, Lu Z. ERK1/2-dependent phosphorylation and nuclear translocation of PKM2 promotes the Warburg effect. *Nat Cell Biol* 2012;14:1295–1304.
37. Yu Z, Zhao X, Huang L, Zhang T, Yang F, Xie L, Song S, Miao P, Zhao L, Sun X, Liu J, Huang G. Proviral insertion in murine lymphomas 2 (PIM2) oncogene phosphorylates pyruvate kinase M2 (PKM2) and promotes glycolysis in cancer cells. *J Biol Chem* 2013;288:35406–35416.
38. Sainz B Jr, Heesch C. Standing out from the crowd: cancer stem cells in hepatocellular carcinoma. *Cancer Cell* 2013;23:431–433.
39. Xu XL, Xing BC, Han HB, Zhao W, Hu MH, Xu ZL, Li JY, Xie Y, Gu J, Wang Y, Zhang ZQ. The properties of tumor-initiating cells from a hepatocellular carcinoma patient’s primary and recurrent tumor. *Carcinogenesis* 2010;31:167–174.
40. Zhang ZQ, Bish LT, Holtzer H, Sweeney HL. Sarcomeric-alpha-actinin defective in vinculin-binding causes Z-line expansion and nemaline-like body formation in cultured chick myotubes. *Exp Cell Res* 2009;315:748–759.
41. Hu Y, Smyth GK. ELDA: extreme limiting dilution analysis for comparing depleted and enriched populations in stem cell and other assays. *J Immunol Methods* 2009;347:70–78.
42. Fernández-Duran I, Quintanilla A, Tarrats N, Birch J, Hari P, Millar FR, Lagnado AB, Smer-Barreto V, Muir M, Brunton VG, Passos JF, Acosta JC. Cytoplasmic innate immune sensing by the caspase-4 non-canonical inflammasome promotes cellular senescence. *Cell Death Differ* 2022;29:1267–1282.

---

Received June 7, 2022. Accepted October 7, 2022.

#### Correspondence

Zhiqian Zhang, PhD, Peking University Cancer Hospital, 52 Fucheng Road, Beijing 100142, P.R. China. e-mail: zlzqzhang@bjmu.edu.cn; Dianrong Xiu, MD, Department of General Surgery, Peking University Third Hospital, Beijing, P.R. China e-mail: xiudianrong@163.com; or Yanhua Zhang, Department of Pharmacology, Peking University Cancer Hospital, Beijing, P.R. China. e-mail: zyh8812@163.com.

#### CRediT Authorship Contributions

Zhiqian Zhang, PhD (Conceptualization: Lead; Funding acquisition: Lead; Investigation: Supporting; Methodology: Supporting; Project administration: Lead; Supervision: Lead; Writing – original draft: Lead; Writing – review & editing: Lead)

Jingtao Liu, PhD (Data curation: Equal; Investigation: Lead; Writing – review & editing: Supporting)

Ming Tao, MD (Data curation: Equal; Formal analysis: Equal; Investigation: Equal; Writing – review & editing: Equal)

Wei Zhao, PhD (Data curation: Equal; Formal analysis: Equal; Investigation: Equal; Methodology: Equal; Validation: Equal; Writing – original draft: Equal; Writing – review & editing: Supporting)

Qingru Song, PhD (Investigation: Supporting; Writing – review & editing: Supporting)

Xiaodan Yang, PhD (Formal analysis: Supporting; Investigation: Supporting; Methodology: Supporting; Writing – review & editing: Supporting)

Meng Li, MS (Formal analysis: Supporting; Investigation: Supporting; Project administration: Supporting; Validation: Supporting; Writing – review & editing: Supporting)

Yanhua Zhang, MS (Resources: Equal; Supervision: Supporting; Writing – review & editing: Supporting)

Dianrong Xiu, MD (Investigation: Equal; Resources: Lead; Supervision: Lead; Writing – review & editing: Supporting)

#### Conflicts of interest

These authors disclose the following: W.Z. and Z.Z. own the patent for 1B50-1 antibody. The remaining authors disclose no conflicts.

#### Funding

Supported by National Key Research and Development Program of China (grant no. 2021YFA1300604), the National Natural Science Foundation of China (nos. 81730075, 82030080, and 81872025), the Pilot Project (4th Round) to Reform Public Development of Beijing Municipal Medical Research Institute (2021-1), and the “Beijing Authority of Hospitals” Mission Plan (no: SML20191101).